Available online at www.sciencedirect.com
SCIENCE DIRECT®
Journal of Computational Physics 204 (2005) 633–665
JOURNAL OF COMPUTATIONAL PHYSICS
www.elsevier.com/locate/jcp

Metric tensors for anisotropic mesh generation

Weizhang Huang *

Department of Mathematics, The University of Kansas, 405 Snow Hall, Lawrence, KS 66045, USA

Received 11 November 2003; received in revised form 12 October 2004; accepted 20 October 2004
Available online 30 November 2004

Abstract

It has been amply demonstrated that significant improvements in accuracy and efficiency can be gained when a properly chosen anisotropic mesh is used in the numerical solution for a large class of problems which exhibit anisotropic solution features. In practice, an anisotropic mesh is commonly generated as a quasi-uniform mesh in the metric determined by a tensor specifying the shape, size, orientation of elements. Thus, it is crucial to choose an appropriate metric tensor for anisotropic mesh generation and adaptation. In this paper, we develop a general formula for the metric tensor for use in any spatial dimension. The formulation is based on error estimates for polynomial preserving interpolation on simiplicial elements. Numerical results in two-dimensions are presented to demonstrate the ability of the metric tensor to produce anisotropic meshes with correct mesh concentration and good overall quality. The procedure developed in this paper for defining the metric tensor can also be applied to other types of error estimates.

MSC: 65M50; 65M60; 65L50; 65L60
Keywords: Anisotropic mesh generation; Mesh adaptation; Equidistribution; Error analysis; Finite element method

1. Introduction

Many physical problems exhibit a common anisotropic feature that their solutions change more significantly in one direction than the others. Examples include those having boundary layers, shock waves, interfaces, and edge singularities. For the numerical solution of this type of problems, it is advantageous to use a properly chosen anisotropic mesh where elements are aligned to the geometry of the solution and can have a large aspect ratio. Compared to traditionally used isotropic ones, anisotropic meshes are more difficult to generate, requiring a full control of both the shape, size, and orientation of elements.

* Tel.: +1 785 864 3651; fax: +1 785 864 5255.
E-mail address: huang@math.ku.edu.

0021-9991/$ - see front matter © 2004 Elsevier Inc. All rights reserved.
doi:10.1016/j.jcp.2004.10.024

In practice, they are commonly generated as quasi-uniform meshes in the metric determined by a tensor (or a matrix-valued function) specifying the shape, size, and orientation of elements on the entire physical domain. Such a metric tensor is often given on a background mesh, either prescribed by the user or chosen as the mesh from the previous iteration in an adaptive solver.

A number of meshing strategies have been developed in the last decade for generating anisotropic meshes according to a given metric tensor. Examples are the Delaunay-type triangulation method [5,6,8,29], the advancing front method [15], the bubble mesh method [34], and the method combining local modification with smoothing or node movement [2,7,13,18,30]. Among these meshing strategies, the metric tensor is commonly defined based on the Hessian of a solution variable and largely motivated by the results of D'Azevedo [10] and D'Azevedo and Simpson [11] on linear interpolation for quadratic functions on triangles. For example, Castro-Díaz et al. [8], Habashi et al. [18], and Remacle et al. [30] define their metric tensor as

$$M = |H(v)| \equiv Q \begin{pmatrix} |\lambda_1| & 0 & 0 \\ 0 & |\lambda_2| & 0 \\ 0 & 0 & |\lambda_3| \end{pmatrix} Q^{\mathrm{T}}, \tag{1}$$

given the eigen-decomposition of the Hessian of function v, $H(v) = Q\,\mathrm{diag}(\lambda_1, \lambda_2, \lambda_3)Q^{\mathrm{T}}$. M in Eq. (1) is further modified by imposing the maximal and minimal edge lengths to guarantee its positive definiteness and avoid unrealistic metric. In his two-dimensional anisotropic mesh generation code BAMG, Hecht [20] uses

$$M = \frac{1}{\epsilon_0 \cdot \mathrm{Coef}^2} \cdot \frac{|H(v)|}{\max\{\mathrm{CutOff}, |v|\}} \tag{2}$$

for the relative error and

$$M = \frac{1}{\epsilon_0 \cdot \mathrm{Coef}^2} \cdot \frac{|H(v)|}{\sup(v) - \inf(v)} \tag{3}$$

for the absolute error, where ϵ_0, Coef, and CutOff are the user specified parameters used for setting the level of the linear interpolation error (with default value 10^{-2}), the value of a multiplicative coefficient on the mesh size (with default value 1), and the limit value of the relative error evaluation (with default value 10^{-5}), respectively. In [16], George and Hecht define the metric tensor for various norms of the interpolation error as

$$M = \left(\frac{c_0}{\epsilon_0}\right)^{v} Q \begin{pmatrix} |\lambda_1|^{v} & 0 & 0 \\ 0 & |\lambda_2|^{v} & 0 \\ 0 & 0 & |\lambda_3|^{v} \end{pmatrix} Q^{\mathrm{T}}, \tag{4}$$

where c_0 is a constant, ϵ_0 is a given error threshold, and $v = 1$ for the L^{∞} norm and the H^1 semi-norm and $v = 1/2$ for L^2 norm of the error. It is emphasized that the definitions (1)–(3) are based on the results of [10] while (4) largely on heuristic considerations.

The objective of this paper is to develop a general formula for the metric tensor for use in anisotropic mesh generation in any spatial dimension. The development is based on the error estimates obtained in the recent work [21] for polynomial preserving interpolation on simplicial elements. These estimates are anisotropic in the sense that they allow a full control of the shape of elements when used within a mesh generation strategy. Compared with the existing anisotropic error estimates (e.g., see [3,14,24,25] and Section 2), the results in [21] have a distinct feature that they are given in terms of a so-called overall mesh quality measure, which in turn is defined through three element-wise quality measures in geometry, alignment, and equidistribution (or adaptation). They shed light on the effects of the mesh qualities on the interpolation error. More importantly, the estimates show that the essence of mesh adaptation is to generate a mesh with good quality in the overall mesh quality measure. The results have been successfully used in [21] to formulate adaptation functionals and the corresponding monitor functions for variational mesh adaptation.

The application of the error estimates of [21] to formulating the metric tensor, M, is relatively straightforward. On the one hand, as a common practice in the existing anisotropic mesh generation codes, we assume that the anisotropic mesh is generated as a quasi-uniform mesh in the metric M, i.e., a mesh where the elements are equilateral (a shape requirement) and unitary in size (a size requirement) in M. On the other hand, the anisotropic mesh is required to have a good quality according to the overall quality measure. This leads to a different set of the shape and size requirements on the mesh elements. Then M is constructed from these requirements.

Let Ω be the bounded physical domain in $\Re^n$ ($n \geqslant 1$). Consider functions of the Sobolev space $W^{l,p}(\Omega)$ for some integer $1 \leqslant l \leqslant k+1$ and real number $p \geqslant 1$, where k is the degree of interpolation polynomials and l and p are related to the regularity of the solution of the partial differential equation at hand. If the interpolation error is measured in the semi-norm of $W^{m,q}(\Omega)$ with $0 \leqslant m \leqslant l$ and $q \geqslant 1$, the metric tensor is given in a continuous form in Eq. (68) for functions in $W^{1,p}(\Omega)$ or in Eq. (70) for functions in $W^{l,p}(\Omega)$ with $l \geqslant 2$ in terms of a prescribed number of elements, N, or in Eq. (69) or (71) in terms of a prescribed error level, ϵ_0. These definitions are general, valid for any $W^{m,q}$ semi-norm of interpolation error and n spatial dimensions. For the commonly used case $l = 2$ (e.g., for linear interpolation), when emphasis is given to mesh alignment and equidistribution, the metric tensor reads as

$$M(\boldsymbol{x}) = \left(\frac{N}{\sigma}\right)^{\frac{2}{n}} \det\left(I + \frac{1}{\alpha}|H(v)|\right)^{\frac{1}{n}\left(\frac{2}{\gamma}-1\right)} \left[I + \frac{1}{\alpha}|H(v)|\right], \tag{5}$$

or, in terms of ϵ_0,

$$M_{\epsilon_0}(\boldsymbol{x}) = \left(\frac{1}{\sigma}\cdot\left(\frac{\alpha}{\epsilon_0}\right)^{\frac{n}{2-m}}\right)^{\frac{2}{n}} \det\left(I + \frac{1}{\alpha}|H(v)|\right)^{\frac{1}{n}\left(\frac{2}{\gamma}-1\right)} \left[I + \frac{1}{\alpha}|H(v)|\right], \tag{6}$$

where I is the identity matrix of order n, $H(v)$ is the Hessian of function v, $\gamma = n/q + (2-m)$,

$$\rho(\boldsymbol{x}) = \det\left(I + \frac{1}{\alpha}|H(v)|\right)^{\frac{1}{\gamma}}, \quad \sigma = \int_\Omega \rho(\boldsymbol{x})\,\mathrm{d}\boldsymbol{x},$$

and the positive parameter α is defined through

$$\int_\Omega \rho(\boldsymbol{x})\,\mathrm{d}\boldsymbol{x} = 2^{1+\frac{n(p-1)}{p\gamma}+\max\left\{0,\frac{n}{p\gamma}-1\right\}}|\Omega|.$$

It is noted that Eq. (5) holds for $0 \leqslant m \leqslant l = 2$, whereas (6) is true only for $0 \leqslant m < l = 2$. The definition given in Eq. (5) or (6) depends on the spatial dimension. Interestingly, taking $n = 2$ (in two-dimensions) and $q = 2$ (with the interpolation error being measured in H^m semi-norm), Eq. (6) reduces to

$$M_{\epsilon_0}(\boldsymbol{x}) = \frac{1}{\sigma}\cdot\left(\frac{\alpha}{\epsilon_0}\right) \det\left(I + \frac{1}{\alpha}|H(v)|\right)^{-\frac{1}{6}} \left[I + \frac{1}{\alpha}|H(v)|\right] \tag{7}$$

for the case $m = 0$ and

$$M_{\epsilon_0}(\boldsymbol{x}) = \frac{1}{\sigma}\cdot\left(\frac{\alpha}{\epsilon_0}\right)^2 \left[I + \frac{1}{\alpha}|H(v)|\right] \tag{8}$$

for the case $m = 1$. It is easy to see that the metric tensor defined in Eq. (8) is similar to those given in Eqs. (2) and (3). They differ in the power of ϵ_0 and in that the metric tensor (8) is always positive definite irrespective of the Hessian $H(v)$. On the other hand, the metric tensor (7) has the same power of ϵ_0 as (2) and (3) but includes an extra non-constant factor involving the determinant of matrix $I + (1/\alpha)|H(v)|$. (Numerical results are presented in Section 4, particularly in Figs. 6–8, to show how the interpolation error responds to ϵ_0 on meshes generated using metric tensors (3), (7), and (8).) It is also worth mentioning that definitions (5) and (6) are different from Eq. (4), particularly for the L^2 norm of the error.

The paper is organized as follows. In Section 2, we describe the anisotropic error estimates for polynomial preserving interpolation on simplicial elements and the related mesh quality measures developed in [21]. The formulation of the metric tensor is developed in Section 3. Numerical results are presented in Section 4 for a selection of examples for generating adaptive anisotropic meshes for given functions and for partial differential equations. Finally, conclusions are drawn in Section 5.

2. Anisotropic estimates for interpolation error

In this section, we describe the error estimates for polynomial preserving interpolation on simplicial elements and the related mesh quality measures developed in [21].

We begin with introducing some notation. Assume that the n-dimensional physical domain Ω is polyhedral and an affine family of triangulations $\{T_h\}$ is given thereon. Then, for each element K, there exists an invertible affine mapping $F_K : \hat{K} \to K$ such that $K = F_K(\hat{K})$, where $\hat{K}$ is the reference element *chosen to be equilateral*. This type of elements are often referred to as simplicial elements in the literature. Denote by $\boldsymbol{\xi} = [\xi_1,\ldots,\xi_n]^T$ the coordinates for $\hat{K}$ and by $\boldsymbol{x} = [x_1,\ldots,x_n]^T$ the local coordinates for K. In the coordinate systems, the affine mapping F_K can be expressed as $\boldsymbol{x} = F_K'\boldsymbol{\xi} + \boldsymbol{c}$, where $\boldsymbol{c}$ is a constant vector and F_K' is the Jacobian matrix. In addition, the lengths of K in the coordinate directions can be written as

$$h_{i,K} = \left(\sum_{j=1}^{n} \left| \frac{\partial x_i}{\partial \xi_j} \right|^2 \right)^{1/2} = \|(F_K')^T \boldsymbol{e}_i\| \quad i = 1,\ldots,n, \tag{9}$$

where $\boldsymbol{e}_i$ is the ith unit vector of the Euclidean space and $\|\cdot\|$ denotes the Euclidean vector norm.

Hereafter, C denotes a generic positive constant. The norm and semi-norm of Sobolev space $W^{m,p}(K)$ are denoted by $\|\cdot\|_{W^{m,p}(K)}$ and $|\cdot|_{W^{m,p}(K)}$, respectively. The *scaled* semi-norm of $W^{m,p}(K)$ is defined as $\langle\cdot\rangle_{W^{m,p}(K)} \equiv |K|^{-1/p}|\cdot|_{W^{m,p}(K)}$, where $|K|$ is the volume of K. Evidently, $\langle v\rangle_{W^{m,p}(K)}$ is an L^p average of $v^{(m)}$ on K.

2.1. Element-wise error estimates

The element-wise error estimates in the following theorem are developed in [21] using the theory of interpolation for finite elements (e.g., see [9]).

Theorem 2.1. *Let $(\hat{K},\hat{P},\hat{\Sigma})$ be a finite element, where $\hat{K}$ is the reference element, $\hat{P}$ is a finite-dimensional linear space of functions defined on $\hat{K}$, and $\hat{\Sigma}$ is a set of degrees of freedom. Let s be the greatest order of partial derivatives occurring in $\hat{\Sigma}$. For some integers m, k, and l: $0 \leqslant m \leqslant l \leqslant k+1$, and some numbers $p,q \in [1,\infty]$, if*

$$W^{l,p}(\hat{K}) \hookrightarrow C^s(\hat{K}), \tag{10}$$

$$W^{l,p}(\hat{K}) \hookrightarrow W^{m,q}(\hat{K}), \tag{11}$$

$$P_k(\hat{K}) \subset \hat{P} \subset W^{m,q}(\hat{K}), \tag{12}$$

then there exists a constant $C = C(\hat{K},\hat{P},\hat{\Sigma})$ such that, for all affine-equivalent finite elements (K,P_K,Σ_K) and $v \in W^{l,p}(K)$

$$|v - \Pi_{k,K}v|_{W^{m,q}(K)} \leqslant C\|(F_K')^{-1}\|^m \cdot |\det(F_K')|^{\frac{1}{q}} \cdot \sum_{i_1,\ldots,i_l} h_{i_1,K}\cdots h_{i_l,K}\left\langle \frac{\partial^l v}{\partial x_{i_1}\cdots\partial x_{i_l}}\right\rangle_{L^p(K)}, \tag{13}$$

where $\Pi_{k,K}$ denotes the kth-degree P_K-interpolation operator on K. Inequality (13) can be written in a different form, viz.,

$$|v - \Pi_{k,K}v|_{W^{m,q}(K)} \leqslant C\|(F_K')^{-1}\|^m \cdot |\det(F_K')|^{\frac{1}{q}} \cdot \left\langle \mathrm{tr}\left((F_K')^{\mathrm{T}}\nabla v\nabla v^{\mathrm{T}}F_K'\right)\right\rangle^{\frac{1}{2}}_{L^{\frac{p}{2}}(K)} \tag{14}$$

for $v \in W^{1,p}(K)$ and

$$|v - \Pi_{k,K}v|_{W^{m,q}(K)} \leqslant C\|(F_K')^{-1}\|^m \cdot \|F_K'\|^{l-2} \cdot |\det(F_K')|^{\frac{1}{q}} \cdot \left\langle \mathrm{tr}\left((F_K')^{\mathrm{T}}|H(D^{l-2}v)|F_K'\right)\right\rangle_{L^p(K)} \tag{15}$$

for $v \in W^{l,p}(K)$ with $l \geqslant 2$, where $\det(\cdot)$ and $\mathrm{tr}(\cdot)$ denote the determinant and the trace of a matrix, respectively, $|H(D^{l-2}v)| \equiv \sum_{i_1,\cdots,i_{l-2}}|H((\partial^{l-2}v)/(\partial x_{i_1}\cdots\partial x_{i_{l-2}}))|$, $H(\cdot)$ is the Hessian of the corresponding function, and $|H(\cdot)| = Q\, diag(|\lambda_1|,\ldots,|\lambda_n|)Q^T$ for a given eigen-decomposition $H(\cdot) = Q\, diag(\lambda_1,\ldots,\lambda_n)Q^{\mathrm{T}}$.

It is remarked that the numbers l and p are related to the regularity of the considered functions. The theorem holds for kth degree interpolation with $k \geqslant 0$ and thus for high order simplicial finite elements. Since the elements are affine, only the Jacobian of the map F_K, F_K', appears in the error estimates. The sufficient conditions for (10) and (11) can be derived from the Embedding Theorem for Sobolev spaces (e.g., see [1]). For the widely used case of Lagrange interpolation ($s = 0$), the conditions $0 \leqslant m \leqslant l \leqslant k + 1$, $1 \leqslant q \leqslant p$, and $l > n/p$ for $p > 1$ or $l \geqslant n$ for $p = 1$ are sufficient for (10) and (11) to hold.

The estimates in Theorem 2.1 are anisotropic. To explain this, we consider the estimate (15) with $l = 2$. Let $Q = [\boldsymbol{q}_1,\ldots,\boldsymbol{q}_n]$. It is not difficult to show

$$\mathrm{tr}\left((F_K')^{\mathrm{T}}|H(v)|F_K'\right) = \sum_i |\lambda_i| \cdot \|(F_K')^{\mathrm{T}}\boldsymbol{q}_i\|^2.$$

Thus, for each i, the length of K in the direction $\boldsymbol{q}_i$, $\|(F_K')^{\mathrm{T}}\boldsymbol{q}_i\|$, can be adjusted according to the eigenvalue λ_i when (15) is used with a meshing strategy. In this sense, estimate (15) provides a separate control of the lengths of K and is anisotropic.

2.2. Mesh quality measures and global error estimates

The results of Theorem 2.1 are now used to define mesh quality measures and develop the global estimate of the interpolation error. An individual element is measured in geometry (or shape), alignment, and equidistribution while the entire mesh is assessed through an overall quality measure.

The geometric quality measure of an element K is defined based on either the Jacobian matrix or its inverse of the affine mapping $F_K : \hat{K} \to K$, viz.,

$$Q_{\mathrm{geo}}(K) = \left[\frac{\mathrm{tr}\left((F_K')^{\mathrm{T}}F_K'\right)}{n\det((F_K')^{\mathrm{T}}F_K')^{\frac{1}{n}}}\right]^{\frac{n}{2(n-1)}} = \left[\frac{\|F_K'\|_{\mathrm{F}}}{\sqrt{n}\det(F_K')^{\frac{1}{n}}}\right]^{\frac{n}{n-1}}, \tag{16}$$

$$\hat{Q}_{\mathrm{geo}}(K) = \left[\frac{\mathrm{tr}\left((F_K')^{-1}(F_K')^{-\mathrm{T}}\right)}{n\det\left((F_K')^{-1}(F_K')^{-\mathrm{T}}\right)^{\frac{1}{n}}}\right]^{\frac{n}{2(n-1)}} = \left[\frac{\|(F_K')^{-1}\|_{\mathrm{F}}}{\sqrt{n}\det(F_K')^{-\frac{1}{n}}}\right]^{\frac{n}{n-1}}, \tag{17}$$

where $\|\cdot\|_{\mathrm{F}}$ is the Frobenius matrix norm. It is remarked that the definition (16) is similar to the shape measure studied by Liu and Joe [27,28] for tetrahedron elements. The ranges of the geometric quality measures are $Q_{\rm geo}(K) \geqslant 1$ and $\hat{Q}_{\rm geo}(K) \geqslant 1$, with the best quality attained by $Q_{\rm geo}(K) = 1$ or $\hat{Q}_{\rm geo}(K) = 1$. From the well known arithmetic-mean geometric-mean inequality it is not difficult to show

$$\left[\frac{1}{n(n-1)}\left(\left(\frac{\mu_{\max}}{\mu_{\min}}\right)^{\frac{1}{2n}}-1\right)^2+1\right]^{\frac{n}{2(n-1)}} \leqslant Q_{\rm geo}(K) \leqslant \frac{\mu_{\max}}{\mu_{\min}},$$

$$\left[\frac{1}{n(n-1)}\left(\left(\frac{\mu_{\max}}{\mu_{\min}}\right)^{\frac{1}{2n}}-1\right)^2+1\right]^{\frac{n}{2(n-1)}} \leqslant \hat{Q}_{\rm geo}(K) \leqslant \frac{\mu_{\max}}{\mu_{\min}},$$

where $\mu_{\min}$ and $\mu_{\max}$ are the minimal and maximal singular values of F'_K. These inequalities imply that $Q_{\rm geo}(K)$ and $\hat{Q}_{\rm geo}(K)$ are equivalent to $\mu_{\max}/\mu_{\min}$ or the aspect ratio of K since n is the number of the dimension and usually small ($n = 2$ or 3).

The definitions of other mesh quality measures and the global error bounds are given in the following theorem [21].

Theorem 2.2. *Suppose that the conditions (10)–(12) of Theorem 2.1 are satisfied. (a) For $v \in W^{1,p}(\Omega)$ and $0 \leqslant m \leqslant 1$,*

$$\left[\sum_K |v - \Pi_{k,K} v|^q_{W^{m,q}(K)}\right]^{\frac{1}{q}} \leqslant C N^{-\frac{1-m}{n}} \sqrt{\alpha_{h,1}}\, Q_{{\rm mesh},h,1}, \tag{18}$$

where N is the number of elements, $\gamma_1 = n/q + (1 - m)$, and

$$Q_{{\rm mesh},h,1} = \left[\frac{1}{\sigma_{h,1}}\sum_K |K|\rho_{K,1}\left(\hat{Q}_{\rm geo}^{\frac{m(n-1)}{n}} Q_{{\rm ali},1}^{\frac{n-1}{n}} Q_{{\rm eq},1}^{\frac{1-m}{n}}\right)^q\right]^{\frac{1}{q}}, \tag{19}$$

$$\sigma_{h,1} = \sum_K |K|\rho_{K,1}, \tag{20}$$

$$Q_{{\rm ali},1}(K) = \left[\frac{\left\langle {\rm tr}\left((F'_K)^{\rm T}\left[I + \frac{1}{\alpha_{h,1}}\nabla v \nabla v^{\rm T}\right] F'_K\right)\right\rangle_{L^{\frac{p}{2}}(K)}}{\left\langle n \det\left((F'_K)^{\rm T}\left[I + \frac{1}{\alpha_{h,1}}\nabla v \nabla v^{\rm T}\right] F'_K\right)^{\frac{1}{n}}\right\rangle_{L^{\frac{p}{2}}(K)}}\right]^{\frac{n}{2(n-1)}}, \tag{21}$$

$$Q_{{\rm eq},1}(K) = \frac{N|K|\rho_{K,1}}{\sigma_{h,1}}, \tag{22}$$

$$\rho_{K,1} = \left\langle 1 + \frac{1}{\alpha_{h,1}}\|\nabla v\|^2\right\rangle^{\frac{1}{2\gamma_1}}_{L^{\frac{p}{2n}}(K)}, \tag{23}$$

$$\alpha_{h,1} = \left[\frac{1}{|\Omega|}\sum_K |K| \langle \|\nabla v\| \rangle^{\frac{1}{\gamma_1}}_{L^{\frac{p}{n}}(K)}\right]^{2\gamma_1}. \tag{24}$$

(*b*) *For* $v \in W^{l,p}(\Omega)$ *with* $l \geqslant 2$ *and* $0 \leqslant m \leqslant l$,

$$\left[\sum_K |v - \Pi_{k,K} v|^q_{W^{m,q}(K)}\right]^{\frac{1}{q}} \leqslant C N^{-\frac{l-m}{n}} \alpha_{h,2} Q_{\mathrm{mesh},h,2}, \tag{25}$$

where $\gamma = n/q + (l - m)$,

$$Q_{\mathrm{mesh},h,2} = \left[\frac{1}{\sigma_{h,2}} \sum_K |K| \rho_{K,2} \left(\hat{Q}_{\mathrm{geo}}^{\frac{m(n-1)}{n}} Q_{\mathrm{geo}}^{\frac{(l-2)(n-1)}{n}} Q_{\mathrm{ali},2}^{\frac{2(n-1)}{n}} Q_{\mathrm{eq},2}^{\frac{l-m}{n}}\right)^q\right]^{\frac{1}{q}}, \tag{26}$$

$$\sigma_{h,2} = \sum_K |K| \rho_{K,2}, \tag{27}$$

$$Q_{\mathrm{ali},2}(K) = \left[\frac{\left\langle \mathrm{tr}\left((F'_K)^{\mathrm{T}}\left[I + \frac{1}{\alpha_{h,2}}\left|H\left(D^{l-2}v\right)\right|\right]F'_K\right)\right\rangle_{L^p(K)}}{\left\langle n \det\left((F'_K)^{\mathrm{T}}\left[I + \frac{1}{\alpha_{h,2}}\left|H\left(D^{l-2}v\right)\right|\right]F'_K\right)^{\frac{1}{n}}\right\rangle_{L^p(K)}}\right]^{\frac{n}{2(n-1)}}, \tag{28}$$

$$Q_{\mathrm{eq},2}(K) = \frac{N|K|\rho_{K,2}}{\sigma_{h,2}}, \tag{29}$$

$$\rho_{K,2} = \left\langle \det\left(I + \frac{1}{\alpha_{h,2}}\left|H\left(D^{l-2}v\right)\right|\right)\right\rangle^{\frac{1}{\gamma}}_{L^{\frac{p}{n}}(K)}, \tag{30}$$

and $\alpha_{h,2}$ *is defined through*

$$\sigma_{h,2} \equiv \sum_K |K| \rho_{K,2} = 2^{1 + \frac{n(p-1)}{p\gamma} + \max\left\{0, \frac{n}{p\gamma} - 1\right\}} |\Omega|. \tag{31}$$

We now take a closer look at the error bounds given in estimates (18) and (25). The parameters $\alpha_{h,1}$ and $\alpha_{h,2}$ play a role of regularization, guaranteeing that the adaptation function ρ_K remains strictly positive irrespective of v and its derivatives. They depend only mildly on the mesh, and are bounded below and above by constants independent of the mesh, i.e., for $q \leqslant p$,

$$\langle \|\nabla v\| \rangle_{L^{\frac{1}{\gamma_1}}(\Omega)} \leqslant \sqrt{\alpha_{h,1}} \leqslant \langle \|\nabla v\| \rangle_{L^{\frac{p}{n}}(\Omega)} \tag{32}$$

and

$$\begin{aligned} \hat{C}\left\langle \det\left(\left|H\left(D^{l-2}v\right)\right|\right)\right\rangle^{\frac{1}{n}}_{L^{\frac{1}{\gamma}}(\Omega)} \leqslant \alpha_{h,2} &\leqslant \frac{1}{n}\left[\frac{1}{|\Omega|}\sum_K |K| \left\langle \mathrm{tr}\left(\left|H\left(D^{l-2}v\right)\right|\right)\right\rangle^{\frac{n}{\gamma}}_{L^p(K)}\right]^{\frac{\gamma}{n}} \\ &\leqslant \frac{1}{n}\left\langle \mathrm{tr}\left(\left|H\left(D^{l-2}v\right)\right|\right)\right\rangle_{L^p(\Omega)}, \end{aligned} \tag{33}$$

where $\hat{C}$ is a positive constant.

The quantity $Q_{\mathrm{mesh},h,1}$ for the case $l = 1$ or $Q_{\mathrm{mesh},h,2}$ for $l \geqslant 2$ is the overall mesh quality measure. (For notational simplicity, $Q_{\mathrm{mesh},h}$ will be used to denote one of them in the following. The same goes for other variables.) It can be shown that the range for the overall quality measure is $Q_{\mathrm{mesh},h} \geqslant 1$, with the best quality being attained at $Q_{\mathrm{mesh},h} = 1$. The overall quality measure is defined through three element-wise quality measures, Q_{geo} (and/or $\hat{Q}_{\mathrm{geo}}$), Q_{ali}, and Q_{eq}.

The alignment quality measure, Q_{ali}, is defined similarly as for the geometric quality measure but depends on v through the matrix $I + (1/\alpha_{h,1})\nabla v \nabla v^{\mathrm{T}}$ or $I + (1/\alpha_{h,2})|H(D^{l-2}v)|$. The range is $Q_{\mathrm{ali}} \geqslant 1$, and $Q_{\mathrm{ali}} = 1$ gives the best alignment. The quantity Q_{ali} characterizes the alignment of the shape of elements with the geometry of the solution. To see this more clearly, we take $Q_{\mathrm{ali},2}(K)$ as an example. Assume that $|H(D^{l-2}v)|$ changes mildly on K so that $Q_{\mathrm{ali},2}(K)$ can be approximated by

$$Q_{\mathrm{ali},2}(K) \approx \left[\frac{\mathrm{tr}\left((F'_K)^{\mathrm{T}} \left[I + \alpha_{h,2}^{-1} |H\left(D^{l-2}v\right)|_K \right] F'_K \right)}{n \det\left((F'_K)^{\mathrm{T}} \left[I + \alpha_{h,2}^{-1} |H\left(D^{l-2}v\right)|_K \right] F'_K \right)^{\frac{1}{n}}} \right]^{\frac{n}{2(n-1)}}, \tag{34}$$

where $|H(D^{l-2}v)|_K$ is a certain average of $|H(D^{l-2}v)|$ on K. Denote the eigen-decomposition of matrix $I + \alpha_{h,2}^{-1} |H(D^{l-2}v)|_K$ by

$$I + \alpha_{h,2}^{-1} |H\left(D^{l-2}v\right)|_K = Q \Sigma Q^{\mathrm{T}} = [\boldsymbol{q}_1 \cdots \boldsymbol{q}_n] \Sigma [\boldsymbol{q}_1 \cdots \boldsymbol{q}_n]^{\mathrm{T}},$$

where $\Sigma = \mathrm{diag}(\sigma_1, \ldots, \sigma_n)$ and $\|\boldsymbol{q}_i\| = 1$, $i = 1, \ldots, n$. It is not difficult to verify

$$\mathrm{tr}\left((F'_K)^{\mathrm{T}} \left[I + \alpha_{h,2}^{-1} |H\left(D^{l-2}v\right)|_K \right] F'_K \right) = \|\Sigma^{1/2} Q^{\mathrm{T}} F'_K\|_{\mathrm{F}}^2 = \sum_{i=1}^{n} \sigma_i \|(F'_K)^{\mathrm{T}} \boldsymbol{q}_i\|^2. \tag{35}$$

We need the following lemma for further derivations.

Lemma 2.1. *For any symmetric positive definite* (*SPD*) *matrix* $A = (a_{ij})$ *of order* m,

$$\det(A) \leqslant \prod_{i=1}^{m} a_{ii}, \tag{36}$$

with equality if and only if *A is diagonal.*

Proof. We prove this lemma by induction. The conclusion is obviously true for $m = 1$. Assume that the conclusion holds for any SPD matrix of order no more than $m - 1$. We need to show that the conclusion is also true for any SPD matrix A of order m. Write A into a block form

$$A = \begin{bmatrix} A_{m-1} & \boldsymbol{v} \\ \boldsymbol{v}^{\mathrm{T}} & a_{mm} \end{bmatrix}.$$

Note that A_{m-1} and A_{m-1}^{-1} are also SPD. By assumption, we have

$$\det(A_{m-1}) \leqslant \prod_{i=1}^{m-1} a_{ii}, \tag{37}$$

with equality if and only if A_{m-1} is diagonal. Taking determinant of both sides of the equality

$$\begin{bmatrix} I_{m-1} & 0 \\ -\boldsymbol{v}^{\mathrm{T}} A_{m-1}^{-1} & 1 \end{bmatrix} \begin{bmatrix} A_{m-1} & \boldsymbol{v} \\ \boldsymbol{v}^{\mathrm{T}} & a_{mm} \end{bmatrix} = \begin{bmatrix} A_{m-1} & \boldsymbol{v} \\ 0 & a_{mm} - \boldsymbol{v}^{\mathrm{T}} A_{m-1}^{-1} \boldsymbol{v} \end{bmatrix}$$

and using inequality (37) we get

$$\det(A) = \left(a_{mm} - \boldsymbol{v}^{\mathrm{T}} A_{m-1}^{-1} \boldsymbol{v}\right) \det(A_{m-1}) \leqslant \left(a_{mm} - \boldsymbol{v}^{\mathrm{T}} A_{m-1}^{-1} \boldsymbol{v}\right) \prod_{i=1}^{m-1} a_{ii} \leqslant \prod_{i=1}^{m} a_{ii},$$

where we have used $\boldsymbol{v}^{\mathrm{T}} A_{m-1}^{-1} \boldsymbol{v} \geqslant 0$. Thus, (36) holds. The equal sign in (36) holds if and only if A_{m-1} is diagonal and $\boldsymbol{v}^{\mathrm{T}} A_{m-1}^{-1} \boldsymbol{v} = 0$, with the latter implying $v = 0$. Thus, A is diagonal. □

Take $A = Q^{\mathrm{T}} F'_K (F'_K)^{\mathrm{T}} Q$. It is not difficult to show

$$a_{ii} \equiv \left(Q^{\mathrm{T}} F'_K (F'_K)^{\mathrm{T}} Q \right)_{ii} = \| (F'_K)^{\mathrm{T}} \boldsymbol{q}_i \|^2 \quad i = 1, \ldots, n. \tag{38}$$

Then, the lemma yields

$$\det(F'_K)^2 \leqslant \prod_{i=1}^{n} \| (F'_K)^{\mathrm{T}} \boldsymbol{q}_i \|^2$$

and

$$\det \left((F'_K)^{\mathrm{T}} \left[I + \alpha_{h,2}^{-1} |H(D^{l-2} v)|_K \right] F'_K \right) = \det(F'_K)^2 \prod_{i=1}^{n} \sigma_i \leqslant \prod_{i=1}^{n} \sigma_i \| (F'_K)^{\mathrm{T}} \boldsymbol{q}_i \|^2. \tag{39}$$

Combining this with Eq. (35), we get

$$\frac{\mathrm{tr}\left((F'_K)^{\mathrm{T}} \left[I + \alpha_{h,2}^{-1} |H(D^{l-2} v)|_K \right] F'_K \right)}{n \det \left((F'_K)^{\mathrm{T}} \left[I + \alpha_{h,2}^{-1} |H(D^{l-2} v)|_K \right] F'_K \right)^{\frac{1}{n}}} \geqslant \frac{\sum_{i=1}^{n} \sigma_i \| (F'_K)^{\mathrm{T}} \boldsymbol{q}_i \|^2}{n \left(\prod_{i=1}^{n} \sigma_i \| (F'_K)^{\mathrm{T}} \boldsymbol{q}_i \|^2 \right)^{\frac{1}{n}}} \geqslant 1. \tag{40}$$

Suppose now that K has a perfect alignment quality, i.e., $Q_{\mathrm{ali},2}(K) = 1$. Combining $Q_{\mathrm{ali},2}(K) = 1$ with Eqs. (34) and (40), we obtain

$$\sum_{i=1}^{n} \sigma_i \| (F'_K)^{\mathrm{T}} \boldsymbol{q}_i \|^2 \approx n \left(\prod_{i=1}^{n} \sigma_i \| (F'_K)^{\mathrm{T}} \boldsymbol{q}_i \|^2 \right)^{\frac{1}{n}}, \tag{41}$$

and further from (39),

$$\det(F'_K)^2 \approx \prod_{i=1}^{n} \| (F'_K)^{\mathrm{T}} \boldsymbol{q}_i \|^2. \tag{42}$$

From the arithmetic-mean geometric-mean inequality, (41) gives

$$\sigma_1 \| (F'_K)^{\mathrm{T}} \boldsymbol{q}_1 \|^2 \approx \cdots \approx \sigma_n \| (F'_K)^{\mathrm{T}} \boldsymbol{q}_n \|^2. \tag{43}$$

On the other hand, from Lemma 2.1 Eq. (42) implies that the matrix $Q^{\mathrm{T}} F'_K (F'_K)^{\mathrm{T}} Q$ is approximately diagonal, i.e.,

$$Q^{\mathrm{T}} F'_K (F'_K)^{\mathrm{T}} Q \approx \mathrm{diag}(\mu_1, \ldots, \mu_n).$$

Since Q is orthogonal, this indicates that $(\mu_i, \boldsymbol{q}_i)$'s form a complete eigensystem for the matrix $F'_K (F'_K)^{\mathrm{T}}$. Moreover, from Eq. (38) we have $\mu_i \approx \| (F'_K)^{\mathrm{T}} \boldsymbol{q}_i \|^2$ for $i = 1, \ldots, n$. Substituting into (43) gives

$$\sigma_1 \mu_1 \approx \cdots \approx \sigma_n \mu_n. \tag{44}$$

Hence, we have shown that, if K has a perfect alignment quality (i.e., $Q_{\mathrm{ali},2}(K) = 1$), the eigensystem (μ_i, q_i) of $F'_K (F'_K)^{\mathrm{T}}$, and therefore the shape and orientation of element K, are determined by the eigensystem (σ_i, q_i) of the solution dependent matrix $I + \alpha_{h,2}^{-1} |H(D^{l-2} v)|_K$.

The equidistribution quality measure, Q_{eq}, characterizes the relation of the size of elements with the adaptation function ρ_K. Its range is $Q_{\mathrm{eq}} > 0$. The measure is motivated by the equidistribution principle. For instance, $\max_K Q_{\mathrm{eq}}(K) = 1$ leads to the exact equidistribution relation

$$|K| \rho_K = \frac{\sigma_h}{N} \quad \forall K \in T_h.$$

Moreover, the larger $\max_K Q_{eq}(K)$ is, the farther the mesh deviates from satisfying the equidistribution relation.

The effects of the mesh qualities on interpolation error can be clearly seen from estimates (18) and (25). Particularly, $\hat{Q}_{geo}$ (and Q_{geo}), Q_{ali}, and Q_{eq} appear in $Q_{mesh,h}$ as a product, meaning that their effects on the interpolation error compensate for each other. As such, the interpolation error can stay at a low level when smaller elements are worse shaped than larger elements, or well aligned elements are worse shaped than worse aligned elements. Moreover, $Q_{mesh,h}$ is the only factor in the bounds which depends substantially on the mesh. Thus, the essence of mesh adaptation is to generate a mesh having good overall quality in the measure $Q_{mesh,h}$. This idea has been successfully used in [21] to develop adaptation functionals and the corresponding monitor functions for variational mesh adaptation.

To conclude this section, we briefly describe the relation and comparison of the above estimates with some existing ones. A general anisotropic estimate is obtained by Apel and Dobrowolski [4] and Apel [3]. It has a similar form as the estimate (13) but requires the mesh to satisfy the so-called maximal angle and coordinate system conditions. The results of Formaggia and Perotto [14], given in the L^2 and H^1 norm for linear Lagrange interpolation and Crément-type interpolation in two-dimensions, require no such a priori conditions on the mesh. They are formulated in terms of the eigenvalues and eigenvectors of the Jacobian matrix of the affine mapping $F_K : \hat{K} \to K$ (instead of the mapping itself as in the estimates (14) and (15)). It is not difficult to show that the result of [14] for Lagrange interpolation can be derived from (15). A number of a posteriori error estimators for anisotropic refinement have been developed; e.g., see [12,23,25,26,32]. Particularly, Kunert [24–26] and Kunert and Verfeurth [23] introduce the so-called matching functions to measure the correspondence of the mesh to the anisotropic feature of the physical solution, i.e.,

$$m_1(v,T_h) = \frac{1}{|v|_{H^1(\Omega)}} \left(\sum_{K \in T_h} h_{\min,K}^{-2} \sum_{i=1}^{n} \|\boldsymbol{p}_i^T \nabla v\|_{L^2(K)}^2 \right)^{\frac{1}{2}} \quad \forall v \in H^1(\Omega), \tag{45}$$

$$m_2(v,T_h) = \frac{1}{|v|_{H^2(\Omega)}} \left(\sum_{K \in T_h} h_{\min,K}^{-4} \sum_{i,j=1}^{n} \|\boldsymbol{p}_i^T (D^2 v) \boldsymbol{p}_j\|_{L^2(K)}^2 \right)^{\frac{1}{2}} \quad \forall v \in H^2(\Omega), \tag{46}$$

where $\boldsymbol{p}_i$s are an orthogonal set of suitably defined vectors representing the geometry of element K, $h_{i,K} = \|\boldsymbol{p}_i\|$, and $h_{\min,K} = \min_i h_{i,K}$. A priori and a posteriori error bounds for linear elements are then obtained in terms of these matching functions. The matching functions m_1 and m_2 play a similar role as $Q_{mesh,h,1}$ and $Q_{mesh,h,2}$, i.e., they measure the overall quality of the mesh. However, the use of $|v|_{H^1(\Omega)}$ in Eq. (45) or $|v|_{H^2(\Omega)}$ in (46) is somewhat arbitrary. Indeed, Kunert [24] observes that $m_1(v,T_h)$ can be small and large for mis-adapted meshes. On the contrary, a small value of $Q_{mesh,h}$ always means a good quality of the mesh [21].

3. Metric tensors for anisotropic mesh adaptation

We now use the results of Theorem 2.2 to develop a formula for the metric tensor. Although mainly concerned with anisotropic mesh generation, for comparison purpose we also record the results for the isotropic case.

As a common practice in anisotropic mesh generation, we assume that the metric tensor, denoted by $M(\boldsymbol{x})$, is used in a meshing strategy in such a way that an anisotropic mesh is generated as a quasi-uniform mesh in the metric determined by M. Mathematically, this can be interpreted as the shape and size requirements as follows.

The shape requirement. The elements of the new mesh, T_h, are (or are close to being) equilateral in the metric. Mathematically, this can be expressed as

$$\mathrm{tr}\left((F_K')^{\mathrm{T}} M_K F_K'\right) = n \det\left((F_K')^{\mathrm{T}} M_K F_K'\right)^{\frac{1}{n}} \quad \forall K \in T_h, \tag{47}$$

where M_K is an average of $M(\boldsymbol{x})$ on element K.

The size requirement. The elements of the new mesh T_h have a unitary volume in the metric, viz.,

$$\int_K \sqrt{\det(M(\boldsymbol{x}))}\,\mathrm{d}\boldsymbol{x} = 1 \quad \forall K \in T_h, \tag{48}$$

or, in a discrete form

$$|K|\sqrt{\det(M_K)} = 1 \quad \forall K \in T_h. \tag{49}$$

It is interesting to point out that $\sqrt{\det(M(\boldsymbol{x}))}$ can often be interpreted as an "error" density function. In this interpretation, Eq. (48) implies that the error is evenly distributed or equidistributed among elements. We note that the shape requirement is implemented very much the same way in the existing algorithms and codes. However, the size requirement may vary slightly from code to code. For example, Habashi et al. [18] consider the error equidistribution among edges instead of elements.

It is emphasized that the above shape and size requirements show how the metric tensor M is used within a meshing strategy and are insufficient for its determination. We use the results of Theorem 2.2 to determine M. The idea is to require the new mesh to have a good overall quality in the sense that $Q_{\mathrm{mesh},h}$ is minimized or at least bounded by a reasonably small number. The procedure is to derive conditions from this quality requirement and compare them with Eqs. (47) and (48). We now proceed in two separate cases $l = 1$ and $l \geqslant 2$.

3.1. Case $l = 1$

According to Theorem 2.2 the new mesh should be chosen to have the best overall quality and attain the smallest error bound. However, this optimal mesh is often difficult to obtain numerically by direct minimization because $Q_{\mathrm{mesh},h,1}$ is highly non-linear and non-convex and its minimization often leads to a nasty optimization problem. Here, we use an indirect approach. Recalling that $Q_{\mathrm{mesh},h,1} \geqslant 1$ and the best overall quality is attained at $Q_{\mathrm{mesh},h,1} = 1$, we could ideally require the mesh to satisfy

$$\max_K \hat{Q}_{\mathrm{geo}}(K) = 1, \quad \max_K Q_{\mathrm{ali},1}(K) = 1, \quad \max_K Q_{\mathrm{eq},1}(K) = 1 \tag{50}$$

and thus have

$$Q_{\mathrm{mesh},h,1} \leqslant \left[\max_K \hat{Q}_{\mathrm{geo}}(K)\right]^{\frac{m(n-1)}{n}} \left[\max_K Q_{\mathrm{ali},1}(K)\right]^{\frac{n-1}{n}} \left[\max Q_{\mathrm{eq},1}(K)\right]^{\frac{1-m}{n}} = 1. \tag{51}$$

Unfortunately, such a mesh does not exist in general since the first and second conditions of (50) contradict each other: The first condition requires the elements to be equilateral in the Euclidean metric whereas the second one requires them to be so in the metric proportional to $[I + (1/\alpha_{h,1})\nabla v \nabla v^T]$. In the following, we define the needed metric tensor by compromising these conditions.

We first consider the second and third conditions

$$\max_K Q_{\mathrm{ali},1}(K) = 1, \quad \max_K Q_{\mathrm{eq},1}(K) = 1. \tag{52}$$

The condition $\max_K Q_{\mathrm{ali},1}(K) = 1$ gives

$$\left\langle \mathrm{tr}\left((F_K')^{\mathrm{T}}\left[I + \frac{1}{\alpha_{h,1}}\nabla v \nabla v^{\mathrm{T}}\right] F_K'\right)\right\rangle_{L^{\frac{p}{2}}(K)} = \left\langle n \det\left((F_K')^{\mathrm{T}}\left[I + \frac{1}{\alpha_{h,1}}\nabla v \nabla v^{\mathrm{T}}\right] F_K'\right)^{\frac{1}{n}}\right\rangle_{L^{\frac{p}{2}}(K)} \quad \forall K \in T_h. \tag{53}$$

To be able to compare Eq. (53) with (47), we assume that ∇v and therefore the matrix $I + (1/\alpha_{h,1})\nabla v \nabla v^T$ do not change dramatically on K. Recalling that a scaled Sobolev semi-norm is an average, we can approximate Eq. (53) by

$$\mathrm{tr}\left((F'_K)^{\mathrm{T}}\left[I + \frac{1}{\alpha_{h,1}}\nabla v(\boldsymbol{x})\nabla v(\boldsymbol{x})^{\mathrm{T}}\right]F'_K\right) \approx n\,\det\left((F'_K)^{\mathrm{T}}\left[I + \frac{1}{\alpha_{h,1}}\nabla v(\boldsymbol{x})\nabla v(\boldsymbol{x})^{\mathrm{T}}\right]F'_K\right)^{\frac{1}{n}}. \tag{54}$$

On the other hand, we have from (47)

$$\mathrm{tr}\left((F'_K)^{\mathrm{T}}M(\boldsymbol{x})F'_K\right) \approx n\,\det\left((F'_K)^{\mathrm{T}}M(\boldsymbol{x})F'_K\right)^{\frac{1}{n}} \quad \forall \boldsymbol{x} \in K. \tag{55}$$

By comparing (55) with (54), we obtain

$$M(\boldsymbol{x}) = \theta(\boldsymbol{x})\left[I + \frac{1}{\alpha_{h,1}}\nabla v \nabla v^{\mathrm{T}}\right], \tag{56}$$

where $\theta(\boldsymbol{x})$ is a scalar function which we now determine by using Eq. (49) and the second condition in Eq. (52). Recall that $\max_K Q_{\mathrm{eq}}(K) = 1$ leads to the exact equidistribution relation, i.e.,

$$|K|\rho_{K,1} = \frac{\sigma_{h,1}}{N} \quad \forall K \in T_h.$$

Eliminating $|K|$ from this and Eq. (49), we get

$$\rho_{K,1}\det(M_K)^{-\frac{1}{2}} = \frac{\sigma_{h,1}}{N}. \tag{57}$$

We approximate this by

$$\rho_{K,1}\det(M(\boldsymbol{x}))^{-\frac{1}{2}} \approx \frac{\sigma_{h,1}}{N}$$

and equation (23) by

$$\rho_{K,1} \approx \left(1 + \frac{1}{\alpha_{h,1}}\|\nabla v\|^2\right)^{\frac{1}{2\gamma_1}}.$$

Combining these with Eq. (56), we get

$$\theta = \left(\frac{N}{\sigma_{h,1}}\right)^{\frac{2}{n}}\left(1 + \frac{1}{\alpha_{h,1}}\|\nabla v\|^2\right)^{\frac{1}{n}\left(\frac{1}{\gamma_1}-1\right)}. \tag{58}$$

Substituting this into Eq. (56), we get the metric tensor for the case $l = 1$ as

$$M(\boldsymbol{x}) = \left(\frac{N}{\sigma_{h,1}}\right)^{\frac{2}{n}}\left(1 + \frac{1}{\alpha_{h,1}}\|\nabla v\|^2\right)^{\frac{1}{n}\left(\frac{1}{\gamma_1}-1\right)}\left[I + \frac{1}{\alpha_{h,1}}\nabla v \nabla v^{\mathrm{T}}\right] \quad \boldsymbol{x} \in K, \tag{59}$$

where N is the number of elements. If we further replace $\sigma_{h,1}$ and $\alpha_{h,1}$ by their continuous counterparts,

$$\alpha_1 = \left[\frac{1}{|\Omega|}\int_\Omega \|\nabla v\|^{\frac{1}{\gamma_1}}\,\mathrm{d}\boldsymbol{x}\right]^{2\gamma_1}, \tag{60}$$

$$\sigma_1 = \int_\Omega \rho_1(\boldsymbol{x})\,\mathrm{d}\boldsymbol{x}, \tag{61}$$

$$\rho_1 = \left(1 + \frac{1}{\alpha_1}\|\nabla v\|^2\right)^{\frac{1}{2\gamma_1}}, \tag{62}$$

from the alignment and equidistribution requirements (52) we obtain the metric tensor in a continuous form as

$$M_{\text{ali},1,N}(\boldsymbol{x}) = \left(\frac{N}{\sigma_1}\right)^{\frac{2}{n}}\left(1 + \frac{1}{\alpha_1}\|\nabla v\|^2\right)^{\frac{1}{n}\left(\frac{1}{\gamma_1}-1\right)}\left[I + \frac{1}{\alpha_1}\nabla v \nabla v^{\mathrm{T}}\right] \quad \forall \boldsymbol{x} \in \Omega. \tag{63}$$

Sometimes it is more convenient to use a prescribed error level instead of N. Consider the situation where a level, ϵ_0, is given for the $W^{m,q}$ semi-norm of interpolation error. Assuming that $Q_{\text{mesh},h,1}$ is bounded by a reasonably small number, estimate (18) implies that the global error bound is proportional to $N^{-(1-m)/n}\sqrt{\alpha_1}$. Setting this equal to ϵ_0, we get for $m = 0$

$$N = \left(\frac{\sqrt{\alpha_1}}{\epsilon_0}\right)^{\frac{n}{1-m}}.$$

Substituting it into Eq. (63) yields

$$M_{\text{ali},1,\epsilon_0}(\boldsymbol{x}) = \left(\frac{1}{\sigma_1}\cdot\left(\frac{\sqrt{\alpha_1}}{\epsilon_0}\right)^{\frac{n}{1-m}}\right)^{\frac{2}{n}}\left(1 + \frac{1}{\alpha_1}\|\nabla v\|^2\right)^{\frac{1}{n}\left(\frac{1}{\gamma_1}-1\right)}\left[I + \frac{1}{\alpha_1}\nabla v \nabla v^{\mathrm{T}}\right] \quad \forall \boldsymbol{x} \in \Omega. \tag{64}$$

Similarly, from the geometric and equidistribution requirements in Eq. (50),

$$\max_K \hat{Q}_{\text{geo}}(K) = 1, \quad \max_K Q_{\text{eq},1}(K) = 1, \tag{65}$$

we can obtain

$$M_{\text{geo},1,N}(\boldsymbol{x}) = I\left(\frac{N}{\sigma_1}\right)^{\frac{2}{n}}\left(1 + \frac{1}{\alpha_1}\|\nabla v\|^2\right)^{\frac{1}{n\gamma_1}} \quad \forall \boldsymbol{x} \in \Omega, \tag{66}$$

$$M_{\text{geo},1,\epsilon_0}(\boldsymbol{x}) = I\left(\frac{1}{\sigma_1}\cdot\left(\frac{\sqrt{\alpha_1}}{\epsilon_0}\right)^{\frac{n}{1-m}}\right)^{\frac{2}{n}}\left(1 + \frac{1}{\alpha_1}\|\nabla v\|^2\right)^{\frac{1}{n\gamma_1}} \quad \forall \boldsymbol{x} \in \Omega. \tag{67}$$

Finally, a metric tensor taking into account the geometry, alignment, and equidistribution qualities of elements can be defined by combining Eqs. (63) and (64),

$$M_{1,N}(\boldsymbol{x}) = \omega M_{\text{geo},1,N}(\boldsymbol{x}) + (1-\omega)M_{\text{ali},1,N}(\boldsymbol{x})$$

or

$$M_{1,N}(\boldsymbol{x}) = \left(\frac{N}{\sigma_1}\right)^{\frac{2}{n}}\left(1 + \frac{1}{\alpha_1}\|\nabla v\|^2\right)^{\frac{1}{n\gamma_1}}\cdot\left\{\omega I + (1-\omega)\left(1 + \frac{1}{\alpha_1}\|\nabla v\|^2\right)^{-\frac{1}{n}}\left[I + \frac{1}{\alpha_1}\nabla v \nabla v^{\mathrm{T}}\right]\right\} \quad \forall \boldsymbol{x} \in \Omega, \tag{68}$$

where N is a prescribed number of elements and $\omega \in [0, 1]$ is a user specified dimensionless parameter used for balancing mesh regularity (or the geometric requirement) and mesh alignment with the physical solution. Evidently, the choice $\omega = 0$ gives emphasis to the alignment requirement while the choice $\omega = 1$ focuses on the geometric requirement in the definition of the metric tensor. Generally speaking, it may be difficult to choose an optimal value for ω, except for the case $m = 0$ when the interpolation error is measured in L^q norm. In this case, $\hat{Q}_{\rm geo}$ does not appear in $Q_{mesh,h,1}$ (see Eq. (19)). As a consequence, only alignment and equidistribution are needed to consider and thus the value $\omega = 0$ should be used.

In terms of the prescribed level of the $W^{m,q}$ semi-norm of interpolation error, ϵ_0, the metric tensor for $m = 0$ is

$$M_{1,\epsilon_0}(\boldsymbol{x}) = \left(\frac{1}{\sigma_1}\cdot\left(\frac{\sqrt{\alpha_1}}{\epsilon_0}\right)^{\frac{n}{1-m}}\right)^{\frac{2}{n}}\left(1+\frac{1}{\alpha_1}\|\nabla v\|^2\right)^{\frac{1}{n\gamma_1}} \cdot\left\{\omega I+(1-\omega)\left(1+\frac{1}{\alpha_1}\|\nabla v\|^2\right)^{-\frac{1}{n}}\left[I+\frac{1}{\alpha_1}\nabla v\nabla v^{\rm T}\right]\right\} \quad \forall \boldsymbol{x}\in\Omega. \tag{69}$$

3.2. Case $l \geqslant 2$

The metric tensor can be defined similarly for the case $l \geqslant 2$. It is given in a continuous form as

$$M_{2,N}(\boldsymbol{x}) = \left(\frac{N}{\sigma_2}\right)^{\frac{2}{n}}\det\left(I+\frac{1}{\alpha_2}|H(D^{l-2}v)|\right)^{\frac{2}{n\gamma}} \cdot\left\{\omega I+(1-\omega)\det\left(I+\frac{1}{\alpha_2}|H(D^{l-2}v)|\right)^{-\frac{1}{n}}\left[I+\frac{1}{\alpha_2}|H(D^{l-2}v)|\right]\right\}, \tag{70}$$

$$M_{2,\epsilon_0}(\boldsymbol{x}) = \left(\frac{1}{\sigma_2}\cdot\left(\frac{\alpha_2}{\epsilon_0}\right)^{\frac{n}{l-m}}\right)^{\frac{2}{n}}\det\left(I+\frac{1}{\alpha_2}|H(D^{l-2}v)|\right)^{\frac{2}{n\gamma}} \cdot\left\{\omega I+(1-\omega)\det\left(I+\frac{1}{\alpha_2}|H(D^{l-2}v)|\right)^{-\frac{1}{n}}\left[I+\frac{1}{\alpha_2}|H(D^{l-2}v)|\right]\right\}, \tag{71}$$

where $\gamma = n/q + (l - m)$, $\omega \in [0,1]$ is a user specified dimensionless parameter, N is the prescribed number of elements, ϵ_0 is the prescribed level of interpolation error in the $W^{m,q}$ semi-norm,

$$\rho_2 = \det\left(I+\frac{1}{\alpha_2}|H(D^{l-2}v)|\right)^{\frac{1}{\gamma}}, \tag{72}$$

$$\sigma_2 = \int_\Omega \rho_2(\boldsymbol{x})\,{\rm d}\boldsymbol{x}, \tag{73}$$

and α_2 is defined by

$$\int_\Omega \rho_2(\boldsymbol{x})\,{\rm d}\boldsymbol{x} = 2^{1+\frac{n(p-1)}{p\gamma}+\max\left\{0,\frac{n}{p\gamma}-1\right\}}|\Omega|. \tag{74}$$

Note that Eq. (70) holds for $0 \leqslant m \leqslant l$, whereas (71) is true only for $0 \leqslant m < l$. Once again, the choices $\omega = 0$ and $\omega = 1$ give emphasis to the alignment and geometric requirements, respectively. For the case $l = 2$ and $m = 0$, the value $\omega = 0$ should be used since both $Q_{\rm geo}$ and $\hat{Q}_{\rm geo}$ do not appear in $Q_{{\rm mesh},h,2}$ (see Eq. (26)) and only alignment and equidistribution are needed to take into account.

It is instructive to see that, taking $n = 2$ (in two-dimensions), $l = 2$, $q = 2$, and $\omega = 0$, Eq. (71) reduces to Eq. (7) for the case $m = 0$ and (8) for $m = 1$.

3.3. Metric tensor for isotropic mesh adaptation: $l \geqslant 1$

The procedure used in the preceding subsections can also be used for isotropic mesh adaptation. For the purpose of comparison, we record the results in this subsection.

Define the adaptation function and the intensity parameter as

$$\rho_{K,3} = \left[1 + \frac{1}{\alpha_h} \langle v \rangle_{W^{l,p}(K)}\right]^{\frac{n}{\gamma}}, \tag{75}$$

$$\alpha_{h,3} = \left[\frac{1}{|\Omega|} \sum_K |K| \langle v \rangle^{\frac{n}{\gamma}}_{W^{l,p}(K)}\right]^{\frac{\gamma}{n}}. \tag{76}$$

The global bound on interpolation error is given by

$$\left[\sum_K |v - \Pi_{k,K} v|^q_{W^{m,q}(K)}\right]^{\frac{1}{q}} \leqslant CN^{-\frac{l-m}{n}} \alpha_{h,3} Q_{\text{mesh},h,3}, \tag{77}$$

where $\gamma = n/q + (l - m)$,

$$Q_{\text{mesh},h,3} = \left[\frac{1}{\sigma_{h,3}} \sum_K |K| \rho_{K,3} \left(\hat{Q}_{\text{geo}}^{\frac{m(n-1)}{n}} Q_{\text{geo}}^{\frac{l(n-1)}{n}} Q_{\text{eq},3}^{\frac{l-m}{n}}\right)^q\right]^{\frac{1}{q}}, \tag{78}$$

$$Q_{\text{eq},3}(K) = \frac{N|K|\rho_{K,3}}{\sigma_{h,3}}. \tag{79}$$

For the current situation, only mesh regularity and equidistribution are needed to consider, and we require the mesh to satisfy $\max_K Q_{\text{geo}}(K) = 1$ and $\max_K Q_{\text{eq}}(K) = 1$. The metric tensor is then defined in a continuous form as

$$M_{3,N}(\boldsymbol{x}) = I\left(\frac{N}{\sigma_3}\right)^{\frac{2}{n}} \left(1 + \frac{1}{\alpha_3} \|D^l v\|\right)^{\frac{2}{\gamma}}, \tag{80}$$

$$M_{3,\epsilon_0}(\boldsymbol{x}) = I\left(\frac{1}{\sigma_3} \cdot \left(\frac{\alpha_3}{\epsilon_0}\right)^{\frac{n}{l-m}}\right)^{\frac{2}{n}} \left(1 + \frac{1}{\alpha_3} \|D^l v\|\right)^{\frac{2}{\gamma}}, \tag{81}$$

where

$$\rho_3 = \left(1 + \frac{1}{\alpha_3} \|D^l v\|\right)^{\frac{n}{\gamma}}, \tag{82}$$

$$\alpha_3 = \left[\frac{1}{|\Omega|} \int_\Omega \|D^l v\|^{\frac{n}{\gamma}} \mathrm{d}\boldsymbol{x}\right]^{\frac{\gamma}{n}}, \tag{83}$$

$$\sigma_3 = \int_\Omega \rho_3(\boldsymbol{x})\, \mathrm{d}\boldsymbol{x}. \tag{84}$$

3.4. Remarks

We now make a few remarks on the formulas for the metric tensor defined in Eqs. (68), (69), (70), (71), (80), and (81).

First, the formulas of the metric tensor depend on several factors, including the function regularity (through parameters l and p), the dimension of space (n), and the norm used to measure interpolation error (m and q).

Second, the formulas have been derived from the requirements on the mesh to be generated. Thus, the metric tensor should be defined on the new mesh. Of course, this is impractical. Nevertheless, we can compute the metric tensor on a background mesh. Because the background mesh is often taken as the current mesh in an iteration process, one can expect that the so-computed mesh tensor should be accurate enough to serve the purpose. Moreover, this is also compatible with the interface of most existing anisotropic mesh generation codes which require the metric tensor to be given on a background mesh.

Third, one may notice that the formulas of the metric tensors involve derivatives (of order $l \leqslant k + 1$) of the physical solution. Generally speaking, one can assume that the nodal values of the solution or their approximations are available, as typically in the numerical solution of partial differential equations. Then, gradient recovery techniques such as those of Zienkiewicz and Zhu [36,37] and Zhang and Naga [35] can be used, although their convergence has been analyzed only on isotropic meshes. In our computations, we use a technique similar to that of [36,37] (see Section 4 for detail).

Fourth, we have so far assumed that the physical solution has only one component. When multi-components are present, a possibility to define the metric tensor is to use the Euclidean norm of the vector-valued solution. Another possibility is to define a metric tensor for each component and then to take the intersection of all the resulting metric tensors. A method for intersecting metric tensors is described in [8]. Consider two $n \times n$ symmetric and semi-positive definite matrices A and B. There exists a non-singular matrix X such that $X^{-1}AX = \text{diag}(a_1,\ldots,a_n)$ and $X^{-1}BX = \text{diag}(b_1,\ldots,b_n)$. Then, the intersection of A and B is defined as $A \cap B \equiv X\,\text{diag}(\max(a_1,b_1),\ldots,\max(a_n,b_n))X^{-1}$. The intersection of more than two matrices can be defined accordingly.

Finally, we note that the metric tensors defined in Eqs. (68), (69), (70), (71), (80), and (81) have a very similar form as the monitor functions derived in [22] for variational mesh adaptation. In fact, the monitor functions can be obtained by dropping the factors involving N or ϵ_0 in the metric tensors. It is also interesting to point out that among the defined metric tensors, the definition (8) is the one closest to the metric tensor (3) used by Hecht in his code BAMG [20]. They both use the Hessian of the solution, but have different powers of ϵ_0. In addition, a regularization (via the parameter α_2) is used in Eq. (8) to guarantee that M_{2,ϵ_0} is always positive definite irrespective of the Hessian.

4. Numerical results

For illustrative purpose, we present some numerical results for five two-dimensional examples, three problems with given analytical solutions and two for steady-state partial differential equations (PDEs). The numerical results are obtained using a c++ code BAMG (Bidimensional Anisotropic Mesh Generator) developed by Hecht [20] with the metric tensors defined in the preceding section. BAMG is a Delaunay-type triangulator which allows the user to supply a metric tensor or a solution defined on a background mesh. Its internal metric tensors are defined in Eqs. (2) and (3). Once the metric is given, BAMG employs five local minimization tools, edge suppression, vertex suppression, vertex addition, edge swapping, and vertex reallocation (barycentering step) to generate the needed anisotropic mesh or the mesh which is isotropic according to the given metric (e.g., see [8]). BAMG is used here in an iterative fashion: Starting from a coarse mesh as shown in Fig. 1, the nodal values of the solution are obtained either from an analytical

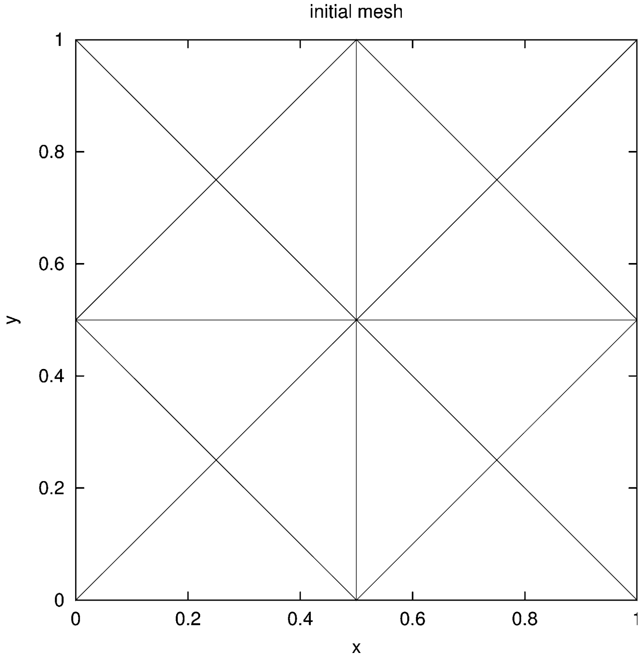

Fig. 1. An initial mesh.

expression (for the problems with given analytical solutions) or by solving a PDE via a finite element method. Having computed the metric tensor, a new mesh is then generated using BAMG. The process is repeated twenty times.

In our computations we use $k = 1$ (for linear interpolation or linear finite elements), $l = 2$, $p = q = 2$, and $m = 0$ (with the error being measured in L^2 norm) or $m = 1$ (with the error being measured in H^1 semi-norm). Unless otherwise stated, $\omega = 0$ is used for computing the metric tensor given in Eqs. (70) and (71), which gives emphasis to alignment. As mentioned in Section 3.2, this is an appropriate choice for the case $m = 0$, where Q_{geo} and $\hat{Q}_{\text{geo}}$ do not appear in the overall mesh quality measure $Q_{\text{mesh},h,2}$ given in Eq. (26). However, it should be pointed out that $\omega = 0$ is not necessarily a good choice in general for the case $m = 1$ where the geometric quality plays a role in the overall mesh quality. We choose $\omega = 0$ mainly because of our interest in anisotropic meshes. But, for comparison purpose we also show numerical results in Fig. 9 for two other values $\omega = 0.1$ and 0.5 for the case $m = 1$.

It is noted that in our computations the solution derivatives used in the metric tensor are approximated using the nodal values of the solution. More specifically, the first-order derivatives are computed using a linear least-squares fitting to the nodal values of the computed solution. The second-order derivatives are obtained in a similar way but based on the nodal values of computed first-order derivatives.

In the results presented below, e denotes the error either for linear interpolation or in the computed linear finite element solution. We use *nbv* and *nbt* to denote the actual numbers of vertices and elements of a mesh, respectively. The quantity *nbt* is different from N used in the formulas of the metric tensor in the previous sections. The former is the actual number of elements in a computed mesh whereas the latter is a prescribed, target number of elements.

It is emphasized that although we use BAMG in our computations, the metric tensors defined in the previous section can also be used with other meshing strategies which employ a metric tensor to specify the shape and size of elements for anisotropic mesh generation.

4.1. Adaptive meshes for given solutions

Example 4.1. The first example is to generate adaptive meshes for

$$v(x,y) = \tanh(60y) - \tanh(60(x-y) - 30) \quad (x,y) \in (0,1) \times (0,1). \tag{85}$$

This function simulates the interaction of a boundary layer with an oblique shock wave, and has been used as a test example for a number of adaptive algorithms; e.g., see [19].

We show in Fig. 2 typical adaptive meshes obtained using $M_{2,N}$ given in Eq. (70) and $M_{3,N}$ in Eq. (80) with $(l,m) = (2,1)$. It can be seen that both metric tensors produce correct mesh concentration. However, the number of elements required to produce the same level of interpolation error is significantly different

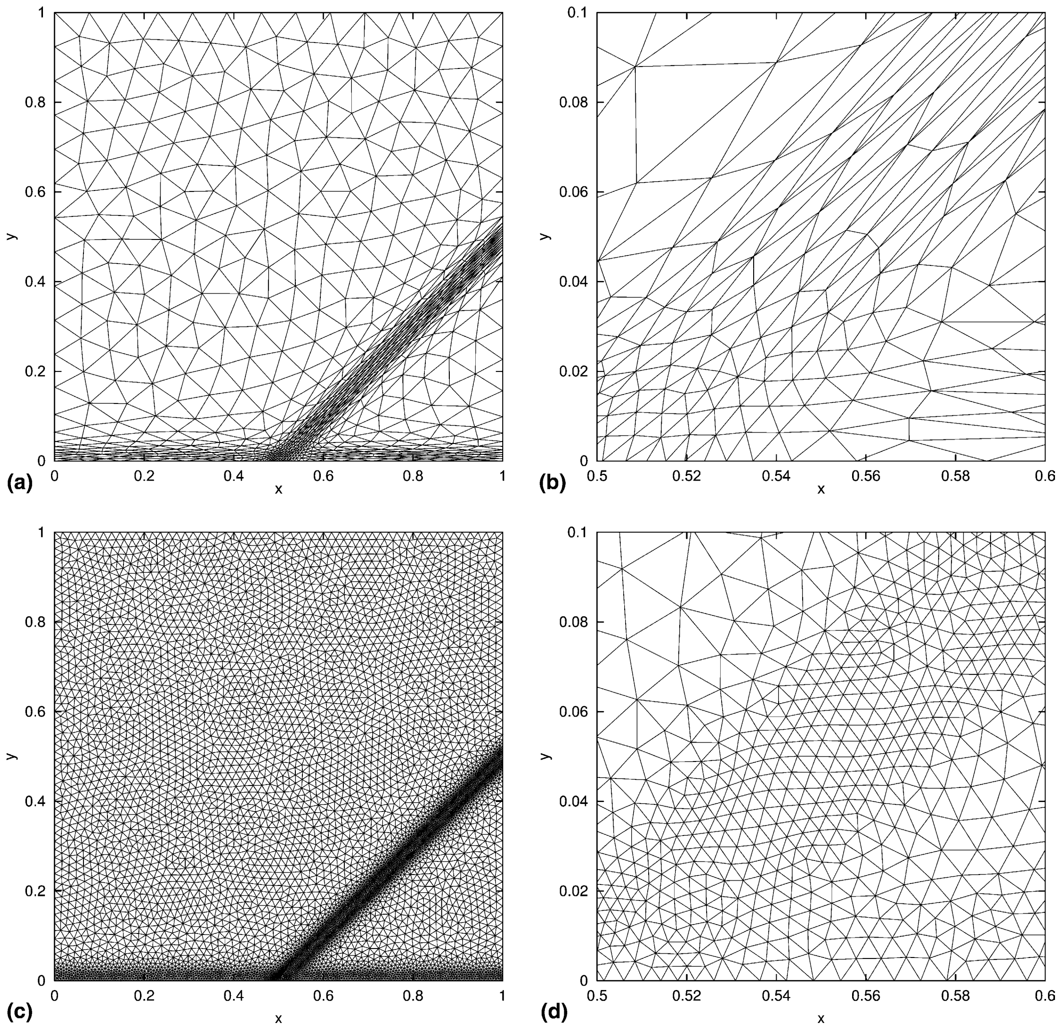

Fig. 2. Example 4.1. (a) An anisotropic mesh obtained with $M_{2,N}$ and $(l,m) = (2,1)$: $nbv = 645$, $nbt = 1187$, $|e|_{H^1} = 0.88$, and $\|e\|_{L^2} = 1.3 \times 10^{-3}$. (b) Close-up of the mesh in (a) near $(x,y) = (0.5,0)$. (c) An isotropic mesh obtained with $M_{3,N}$ and $(l,m) = (2,1)$: $nbv = 7328$, $nbt = 14{,}291$, $|e|_{H^1} = 0.85$, and $\|e\|_{L^2} = 1.0 \times 10^{-3}$. (d): Close-up of the mesh in (c) near $(x,y) = (0.5,0)$.

between isotropic and anisotropic meshes. Indeed, the interpolation error is nearly the same ($|e|_{H^1} \approx 0.88$) for the meshes shown in Fig. 2(a) and (c), but the anisotropic mesh uses only 1187 elements, about a twelfth of the 14291 elements required by the isotropic mesh. The close-ups of both meshes near point $(x,y) = (0.5,0)$ reveal that the elements of the isotropic mesh in the regions of the boundary layer and the shock wave are small and almost equilateral, whereas the anisotropic elements are thin and have a large aspect ratio.

Fig. 3 shows the convergence history for the iteration process of using BAMG with $M_{2,N}$, $(l,m) = (2,1)$, and $N = 500$. One can see that the numbers of vertices (*nbv*) and triangles (*nbt*) and the H^1 semi-norm of the interpolation error stabilize in about five iterations. From this observation, we stop all the computations in 20 iterations, a number sufficiently large to reach a convergent state.

To study the convergence of the interpolation error as the mesh is refined, we plot the L^2 norm and H^1 semi-norm of the error as functions of *nbt* in Fig. 4. For comparison, the results obtained on a uniform mesh are also shown. The convergence is first-order in the H^1 semi-norm (i.e., $|e|_{H^1(\Omega)} = O((nbt)^{-0.5})$) and second-order in the L^2 norm ($\|e\|_{L^2(\Omega)} = O((nbt)^{-1})$) for all methods, confirming the theoretical predictions in Section 3. However, the magnitude of the error is significantly different between the uniform and adaptive meshes. Especially, the decrease of the error from the isotropic adaptive mesh to the anisotropic one is about a factor of 4 in $|\cdot|_{H^1}$ and 10 in $\|\cdot\|_{L^2}$, larger than the decrease from the uniform mesh to the isotropic adaptive one (about a factor of 3 in $|\cdot|_{H^1}$ and 9 in $\|\cdot\|_{L^2}$). This demonstrates the advantage of using a mesh not only adaptive but also well aligned with the solution for solving problems with strong anisotropic features. Interestingly, Fig. 4 also shows that there is no significant difference between the cases $(l,m) = (2,1)$ and $(l,m) = (2,0)$.

The mesh qualities of adaptive meshes are shown in Fig. 5. The maximum norm of the geometric quality measure, $\|Q_{\text{geo}}\|_\infty$, is depicted in Fig. 5(a) as a function of *nbt*. As expected, $\|Q_{\text{geo}}\|_\infty$ is very small (around 2) for isotropic meshes, indicating that their elements are close to being equilateral. This also demonstrates that the code BAMG does a good job in generating a mesh which is isotropic according to a user-supplied metric tensor. On the other hand, the large values of $\|Q_{\text{geo}}\|_\infty$ for anisotropic meshes (around 20 for the case $(l,m) = (2,1)$ and 100 for the case $(l, m) = (2,0)$) mean that some elements have a high aspect ratio. The maximum norms of the alignment and equidistribution quality measures are plotted in Fig. 5(b) and (c),

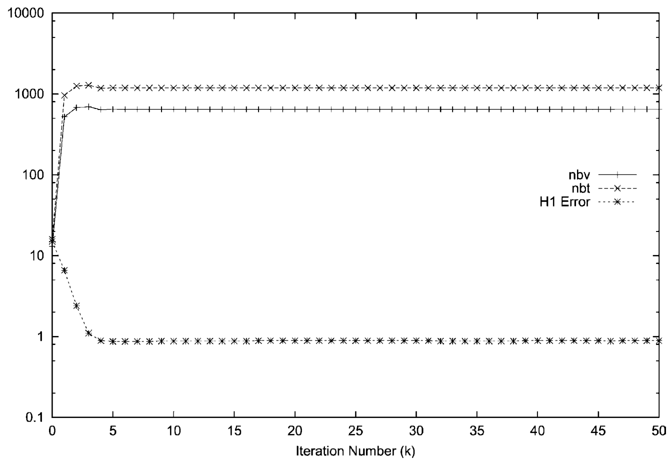

Fig. 3. Example 4.1. Convergence history for the iteration process of using BAMG. The metric tensor $M_{2,N}$ is used with $(l,m) = (2,1)$ and $N = 500$. The curves are shown for *nbv* (the number of the vertices), *nbt* (the number of the triangular elements), and H^1 semi-norm of the interpolation error.

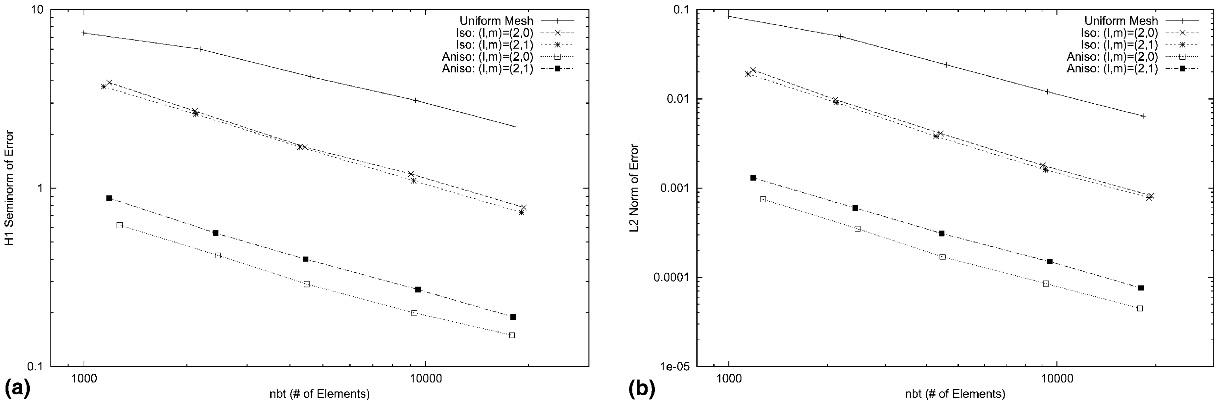

Fig. 4. Example 4.1. The H^1 semi-norm and the L^2 norm of interpolation error are plotted as functions of the number of elements (*nbt*) in (a) and (b), respectively.

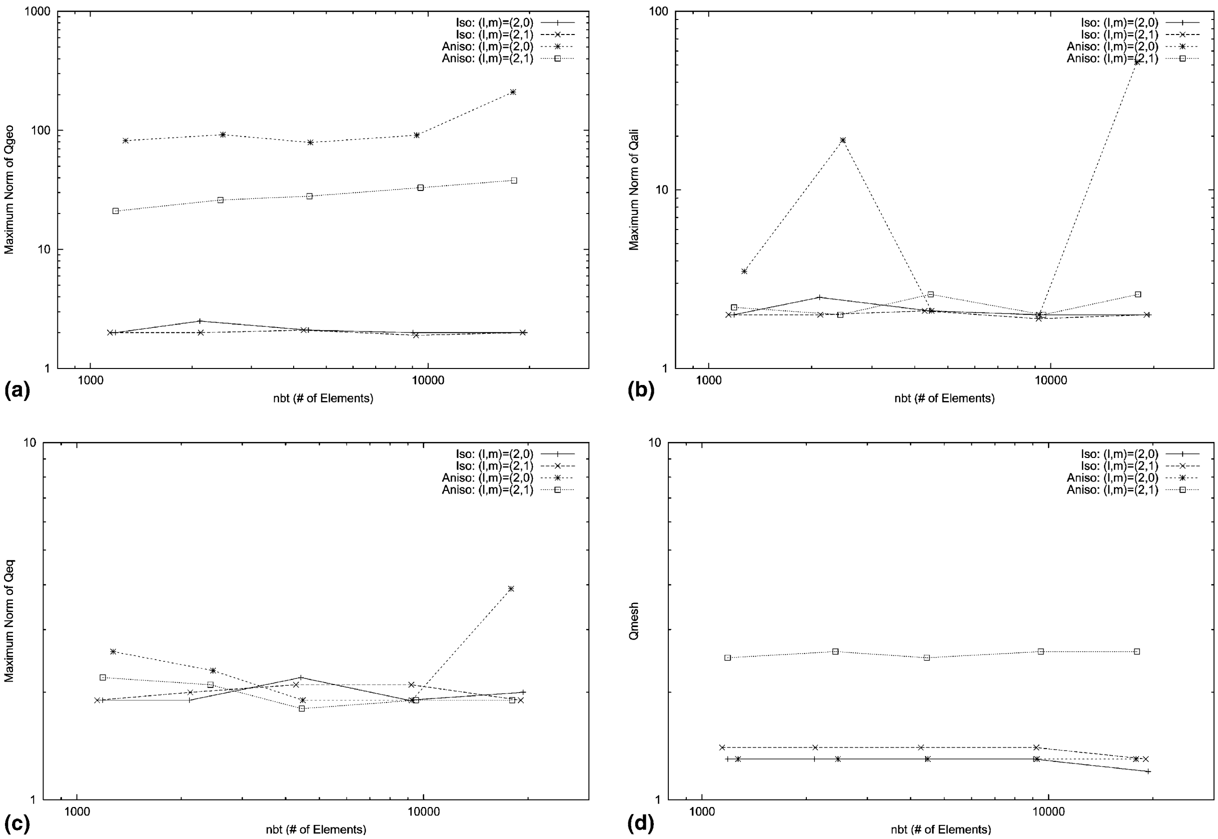

Fig. 5. Example 4.1. The mesh quality measures, $\|Q_{\mathrm{geo}}\|_\infty$, $\|Q_{\mathrm{ali}}\|_\infty$, $\|Q_{\mathrm{eq}}\|_\infty$, and Q_{mesh} are depicted as functions of *nbt* for meshes generated with various metric tensors.

respectively. They show that the mesh is well aligned and adapted to the given metric tensor (and thus the solution) for all but one case with $M_{2,N}$ and $(l,m) = (2,0)$. In this case, $\|Q_{\text{ali}}\|_\infty$ oscillates, with the value ranging from 2 to 50. This happens when some extremely stretched elements are not well aligned with the solution. Fortunately, this does not damage the error and the overall mesh quality because only a few of elements are misaligned and their total area is small. As shown in Fig. 4 and Fig. 5(d), the history of both the error and the overall quality measure is stable as the mesh is refined. In addition, Q_{mesh} is small (with the range from 1.5 to 2.5) for all cases.

We now study the correlations between the prescribed and actual numbers of elements and interpolation error. In Figs. 6 and 7 we show *nbt* as function of N for $M_{2,N}$ and the error as function of ϵ_0 for M_{2,ϵ_0}. It can be seen that, for both cases $m = 0$ and $m = 1$, the actual number of elements (or the error) responds almost linearly to the prescribed, target number of elements (or the prescribed error level). This demonstrates that N (or ϵ_0) in the metric tensor provides a mechanism for effective control of the actual number of elements (or the interpolation error). For comparison purpose, we show in Fig. 8(a) the interpolation error as

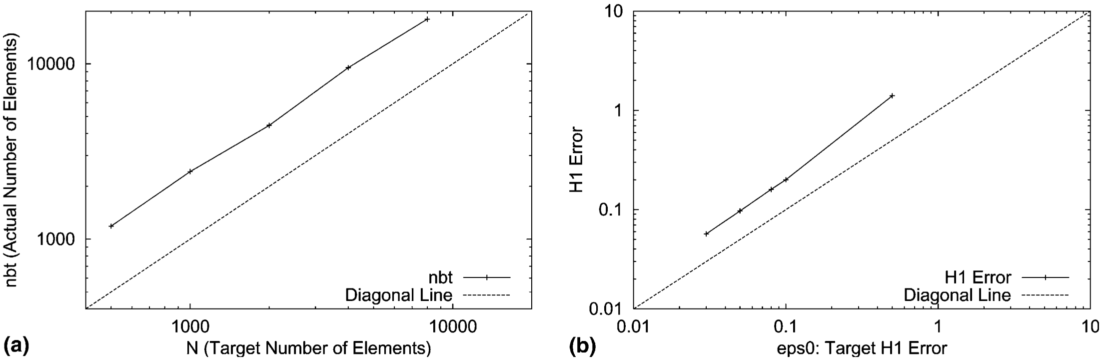

Fig. 6. Example 4.1. Interpolation error is measured in the H^1 semi-norm ($m = 1$). (a) The actual number of elements, *nbt*, is depicted as a function of the target number of elements, N for meshes obtained with the metric tensor $M_{2,N}$ given in Eq. (70). (b) The interpolation error in H^1 semi-norm, $|e|_{H^1(\Omega)}$, is depicted against the prescribed error level, ϵ_0 for meshes obtained with the metric tensor M_{2,ϵ_0} given in Eq. (71) (also see (8)).

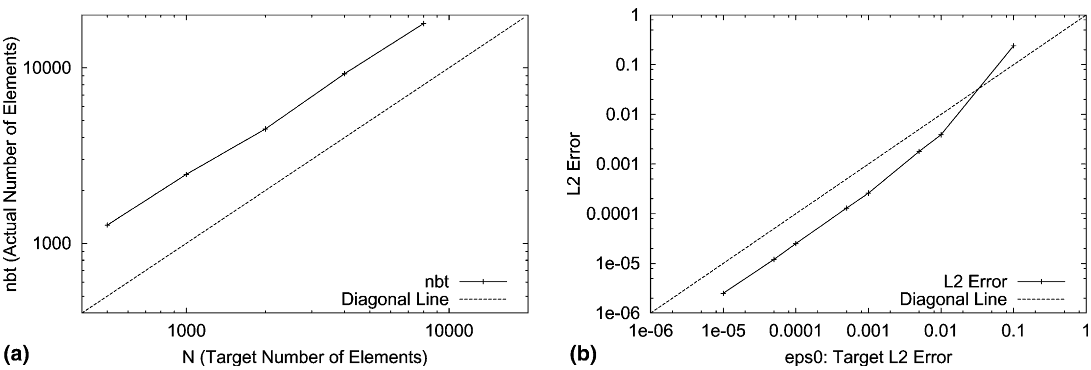

Fig. 7. Example 4.1. Interpolation error is measured in the L^2 norm ($m = 0$). (a) The actual number of elements, *nbt*, is depicted as a function of the target number of elements, N for meshes obtained with the metric tensor $M_{2,N}$ given in Eq. (70). (b) The interpolation error in L^2 semi-norm, $\|e\|_{L^2(\Omega)}$, is depicted against the prescribed error level, ϵ_0 for meshes obtained with the metric tensor M_{2,ϵ_0} given in Eq. (71) (also see (7)).

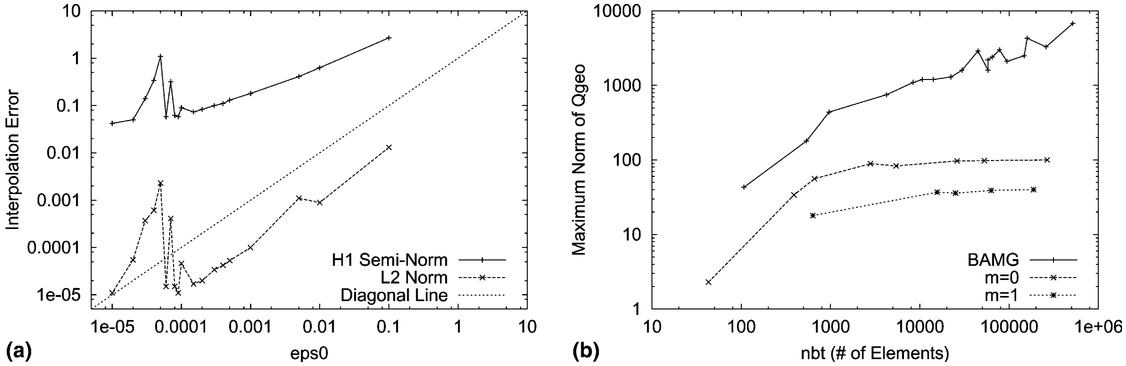

Fig. 8. Example 4.1. (a) Interpolation error in the H^1 semi-norm and L^2 norm is plotted as function of the prescribed error level ϵ_0 for adaptive meshes obtained with the BAMG internal metric tensor defined in Eq. (3). (b) The maximum norm of the geometric quality measure is plotted against the number of elements, *nbt*, as the mesh is refined with metric tensors (3) (BAMG) and (71) with $m = 0$ and $m = 1$ (also see (7) and (8)).

function of ϵ_0 for the BAMG internal metric tensor defined in Eq. (3). It is worth mentioning that the parameter ϵ_0 does not have a clear physical meaning from the construction of (2) and (3) (e.g., see [8]). Fig. 8(a) shows that $|e|_{H^1(\Omega)} \propto \sqrt{\epsilon_0}$ and $\|e\|_{L^2(\Omega)} \propto \epsilon_0$. Thus, ϵ_0 seems to represent the L^2 norm of the error. However, the results also show that the response of the interpolation error to ϵ_0 is not smooth, especially

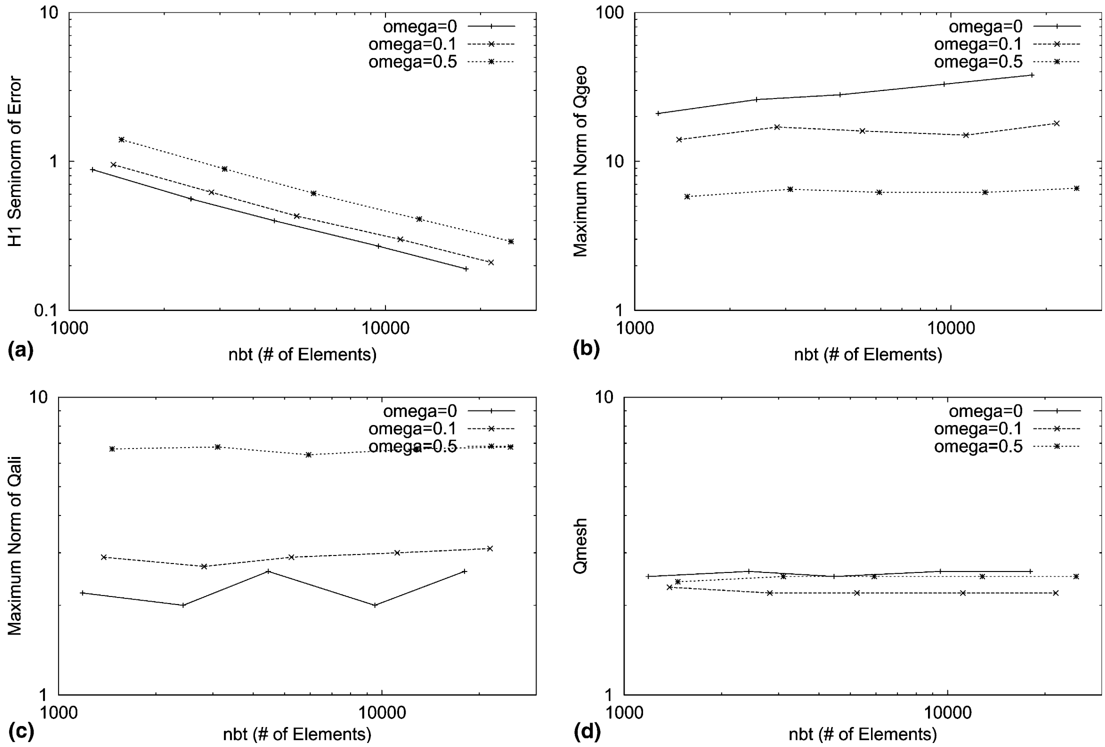

Fig. 9. Example 4.1. Interpolation error in the H^1 semi-norm and mesh quality measures are depicted as functions of *nbt* for adaptive meshes generated with $M_{2,N}$ (see Eq. (70)) with $(l,m) = (2,1)$ and various values of ω.

when ϵ_0 is small. In Fig. 8(b) the maximum norm of the geometric quality measure, $\|Q_{\text{geo}}\|_\infty$, is plotted against the number of elements, *nbt*, as the mesh is refined. Interestingly, the mesh produced with $M_{2,\epsilon}$ plus $m = 0$ or $m = 1$ tends to have a constant $\|Q_{\text{geo}}\|_\infty$. On the contrary, the mesh with the BAMG metric tensor (3) has a rapidly increasing $\|Q_{\text{geo}}\|_\infty$, meaning that some elements are getting more skewed as the mesh is refined. This often is a situation people would like to avoid in mesh generation.

To see the influence of the parameter ω in the metric tensor (70) on the resulting adaptive meshes we plot in Fig. 9 the results obtained with $M_{2,N}$ and three values of ω, 0, 0.1, and 0.5. Fig. 9(a) shows that the difference in $|e|_{H^1(\Omega)}$ is insignificant for these three cases, with the biggest error associated with $\omega = 0.5$ being about twice the smallest one with $\omega = 0.0$. From Figs. 9(b) and (c) one can see that the greater ω is, the smaller $\|Q_{\text{geo}}\|_\infty$ is and the larger $\|Q_{\text{ali}}\|_\infty$. This is consistent with the fact that larger ω gives more emphasis to the geometric requirement and less to the alignment one. The overall mesh quality measure is plotted in Fig. 9(d). Q_{mesh} is small (about 2.5) for all cases. It shows no favor of large or small ω.

Example 4.2. In this example, the function is given by

$$v(x,y) = \tanh\left(-100\left(y - \frac{1}{2} - \frac{1}{4}\sin(2\pi x)\right)^2\right). \tag{86}$$

Compared to Example 4.1, this function has a relatively weaker anisotropic feature. This example is selected to show how much the interpolation error can be improved using an anisotropic mesh over an isotropic one for functions having a mild anisotropic feature.

Two adaptive meshes are shown in Fig. 10. They are obtained using the metric tensors $M_{2,N}$ and $M_{3,N}$ and by adjusting the number of elements such that they give almost the same interpolation error. The anisotropic mesh uses only about one quarter of the elements needed in the isotropic one. The advantage of using anisotropic meshes can also be seen in Fig. 11 where the interpolation error on adaptive and uniform meshes is plotted as function of the number of elements.

The mesh quality measures of adaptive meshes are plotted in Fig. 12. The elements of both isotropic and anisotropic meshes are well aligned and adapted according to the corresponding metric tensors, and the

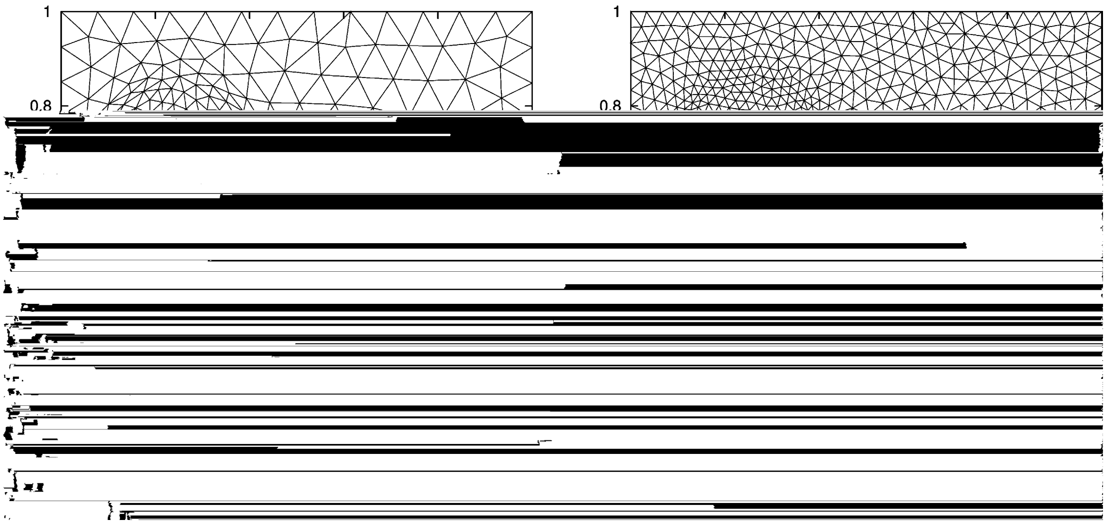

Fig. 10. Example 4.2. (a) An anisotropic mesh obtained with $M_{2,N}$: $nbv = 583$, $nbt = 1094$, $|e|_{H^1} = 0.90$, and $\|e\|_{L^2} = 5.2 \times 10^{-3}$. (b) An isotropic mesh obtained with $M_{3,N}$: $nbv = 2036$, $nbt = 3928$, $|e|_{H^1} = 0.86$, and $\|e\|_{L^2} = 3.8 \times 10^{-3}$.

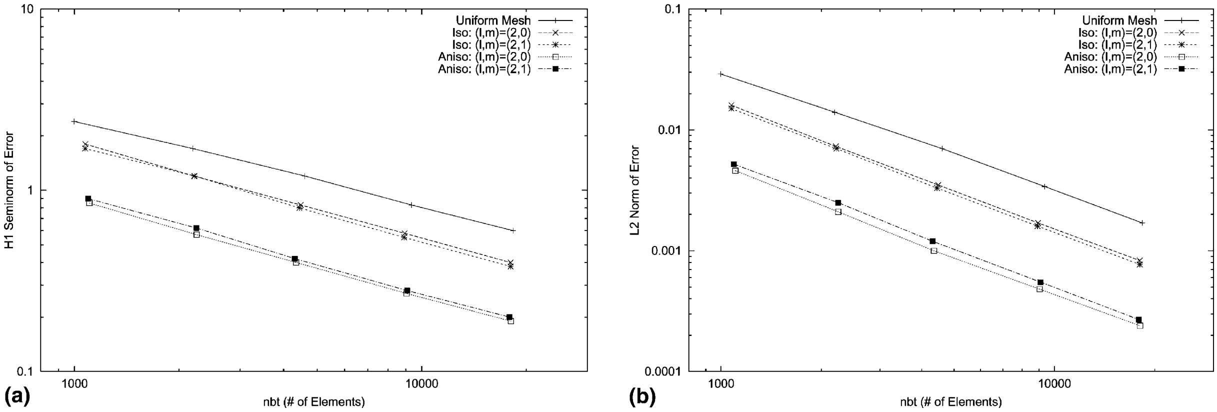

Fig. 11. Example 4.2. The H^1 semi-norm and the L^2 norm are plotted as functions of the number of elements (*nbt*) in (a) and (b), respectively.

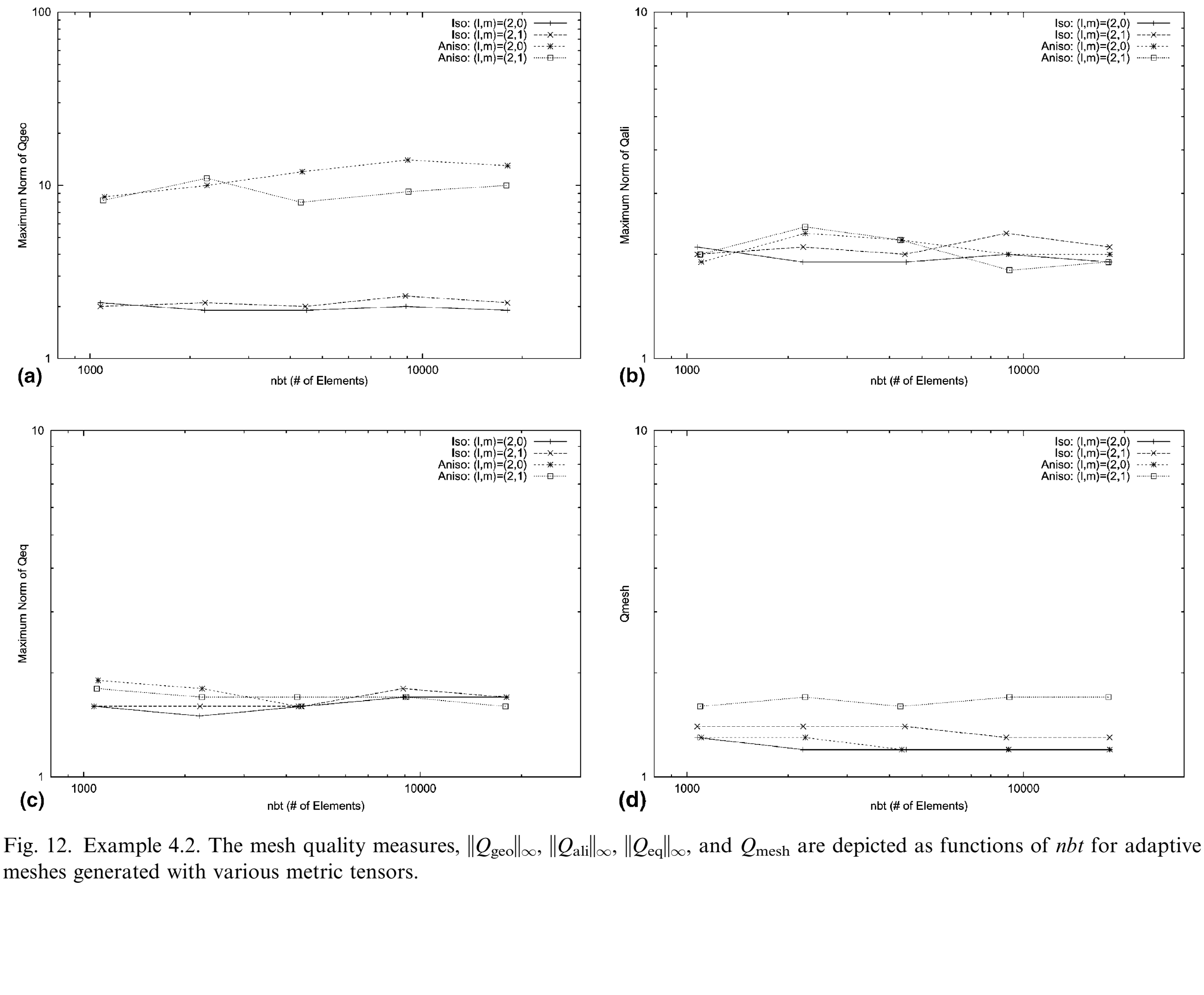

Fig. 12. Example 4.2. The mesh quality measures, $\|Q_{\text{geo}}\|_\infty$, $\|Q_{\text{ali}}\|_\infty$, $\|Q_{\text{eq}}\|_\infty$, and Q_{mesh} are depicted as functions of *nbt* for adaptive meshes generated with various metric tensors.

overall mesh quality is good for all cases. Moreover, Fig. 12(a) shows that some elements of the anisotropic meshes have a large aspect ratio.

Example 4.3. This example is to generate adaptive meshes for

$$v(x,y) = \tanh\left[30\left(x^2+y^2-\frac{1}{8}\right)\right] + \tanh\left[30\left(\left(x-\frac{1}{2}\right)^2+\left(y-\frac{1}{2}\right)^2-\frac{1}{8}\right)\right] + \tanh\left[30\left(\left(x-\frac{1}{2}\right)^2+\left(y+\frac{1}{2}\right)^2-\frac{1}{8}\right)\right] + \tanh\left[30\left(\left(x+\frac{1}{2}\right)^2+\left(y-\frac{1}{2}\right)^2-\frac{1}{8}\right)\right] + \tanh\left[30\left(\left(x+\frac{1}{2}\right)^2+\left(y+\frac{1}{2}\right)^2-\frac{1}{8}\right)\right] \quad (x,y)\in\Omega=(-2,2)\times(-2,2). \tag{87}$$

This function has a more complicated structure than the previous examples and exhibits an isotropic feature. Numerical results are shown in Figs. 13–15. Similar observations as in the previous examples can be made. Especially, the numerical results demonstrate that the metric tensors defined in previous section have the ability to produce adaptive meshes with correct mesh concentration and good overall quality. In addition, the advantage of using an anisotropic mesh is evident even for examples with isotropic features.

4.2. Adaptive solution of partial differential equations

Example 4.4. This example is to solve the boundary value problem of

$$-\epsilon\Delta u + \left(1+e^{\frac{x+y-0.85}{2\epsilon}}\right)^{-1}(u_x+u_y) = -\frac{1}{2\epsilon}\left(1+e^{\frac{x+y-0.85}{2\epsilon}}\right)^{-2} e^{\frac{x+y-0.85}{2\epsilon}} \tag{88}$$

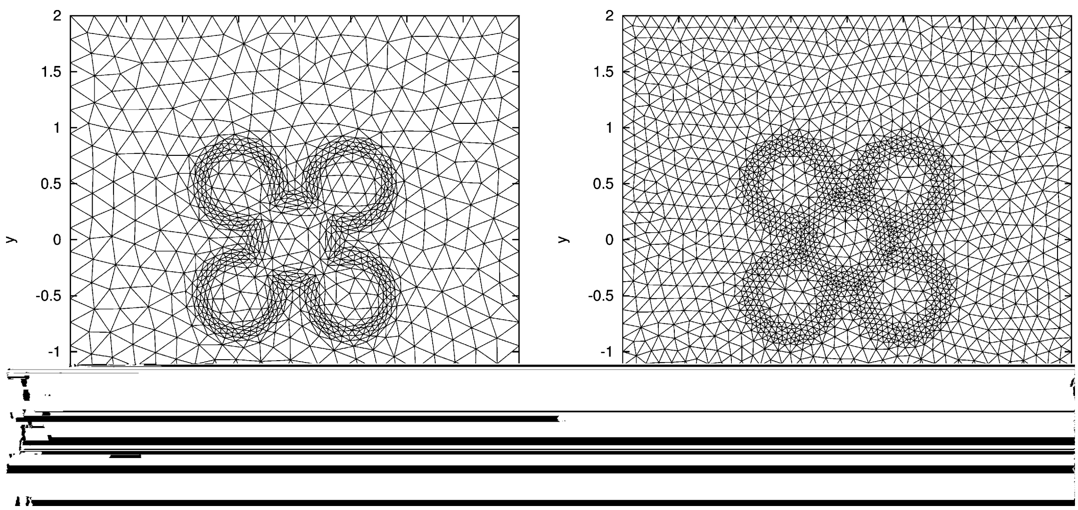

Fig. 13. Example 4.3. (a) An anisotropic mesh obtained with $M_{2,N}$: nbv = 1085, nbt = 2092, $|e|_{H^1} = 3.6$, and $\|e\|_{L^2} = 4.5\times10^{-2}$. (b) An isotropic mesh obtained with $M_{3,N}$: nbv = 2159, nbt = 4188, $|e|_{H^1} = 3.9$, and $\|e\|_{L^2} = 4.9\times10^{-2}$.

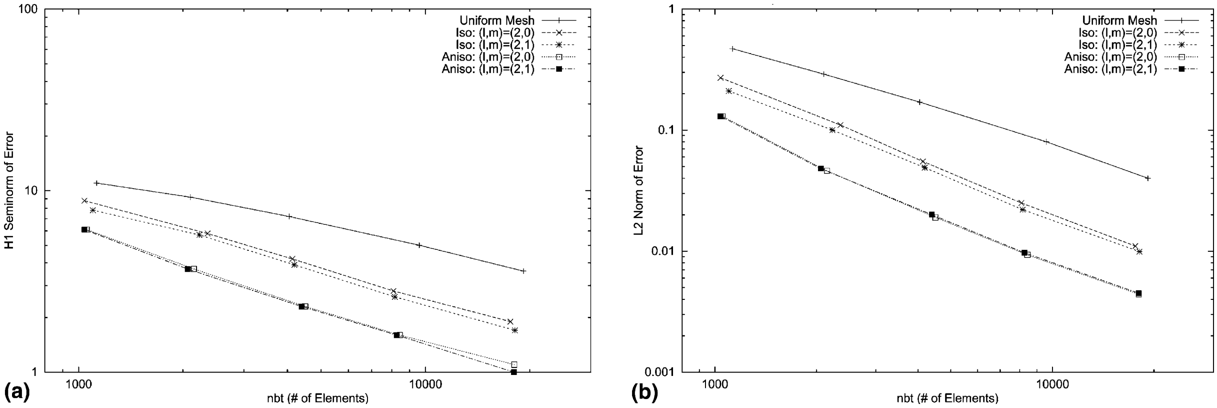

Fig. 14. Example 4.3. The H^1 semi-norm and the L^2 norm are plotted as functions of the number of elements (*nbt*) in (a) and (b), respectively.

on the unit square $\Omega \equiv (0,1) \times (0,1)$. The Dirichlet boundary condition is chosen such that the exact solution is given by

$$u(x,y) = \left(1 + e^{\frac{x+y-0.85}{2\epsilon}}\right)^{-1}. \tag{89}$$

The solution exhibits a sharp layer on line $x + y - 0.85 = 0$ when ϵ is small. In our computations, ϵ is taken as 0.005, and the PDE is discretized on a triangular mesh via linear finite elements. The resulting linear system of algebraic equations is solved using the iterative method BiCGstab2 [17,33] with or without preconditioning. It is emphasized that for this and next examples, the metric tensors are computed using a computed solution of the PDE instead of the exact solution.

Two adaptive meshes of almost the same number of elements are shown in Fig. 16. As for the previous examples with given analytical solutions, both $M_{2,N}$ and $M_{3,N}$ with $(l,m) = (2,1)$ produce correct mesh concentration. However, the anisotropic mesh leads to a much smaller solution error (in either the H^1 semi-norm or the L^2 norm), about a tenth of that on the isotropic mesh. Fig. 17 shows the error as function of the number of elements, confirming again that an anisotropic mesh leads to a much smaller error than an adaptive isotropic one, which in turn improves the accuracy significantly over a uniform mesh.

The mesh qualities of the adaptive meshes are depicted in Fig. 18 as functions of the number of elements. All but the maximum norm of Q_{geo} for the anisotropic mesh are small. The large $\|Q_{\text{geo}}\|_\infty$ indicates that some elements of the anisotropic mesh have a large aspect ratio. This can also be seen in Fig. 16(a) where the elements in the region of the shock wave are thin. Moreover, the small value of Q_{mesh} means that both the isotropic and the anisotropic meshes have a good quality according to their respective metric tensors.

We now study the condition of the coefficient matrix resulting from the linear finite element discretization of PDE (88) on adaptive meshes. The eigenvalues are plotted in Fig. 19 for cases with and without preconditioning. We use here an incomplete LU preconditioner (with level one fill-ins) (e.g., see [31]). It can be seen that the distributions of the eigenvalues are similar for both anisotropic and isotropic meshes, although more scattered for the former. The preconditioner is effective for both cases, with most eigenvalues being clustered around real number 1. The number of BiCGstab2 iterations required to reduce the residual to a level of 10^{-10} is plotted in Fig. 20(a). Without preconditioning, the number grows at a rate of $(nbt)^{0.5}$ initially and then slows down for large *nbt* at the rate $(nbt)^{0.25}$ for the anisotropic mesh, whereas the growth rate is only $(nbt)^{0.25}$ for the isotropic one. On the other hand, with the ILU preconditioning the required number of iterations for both cases is reduced dramatically (with a growth rate $(nbt)^{0.5}$).

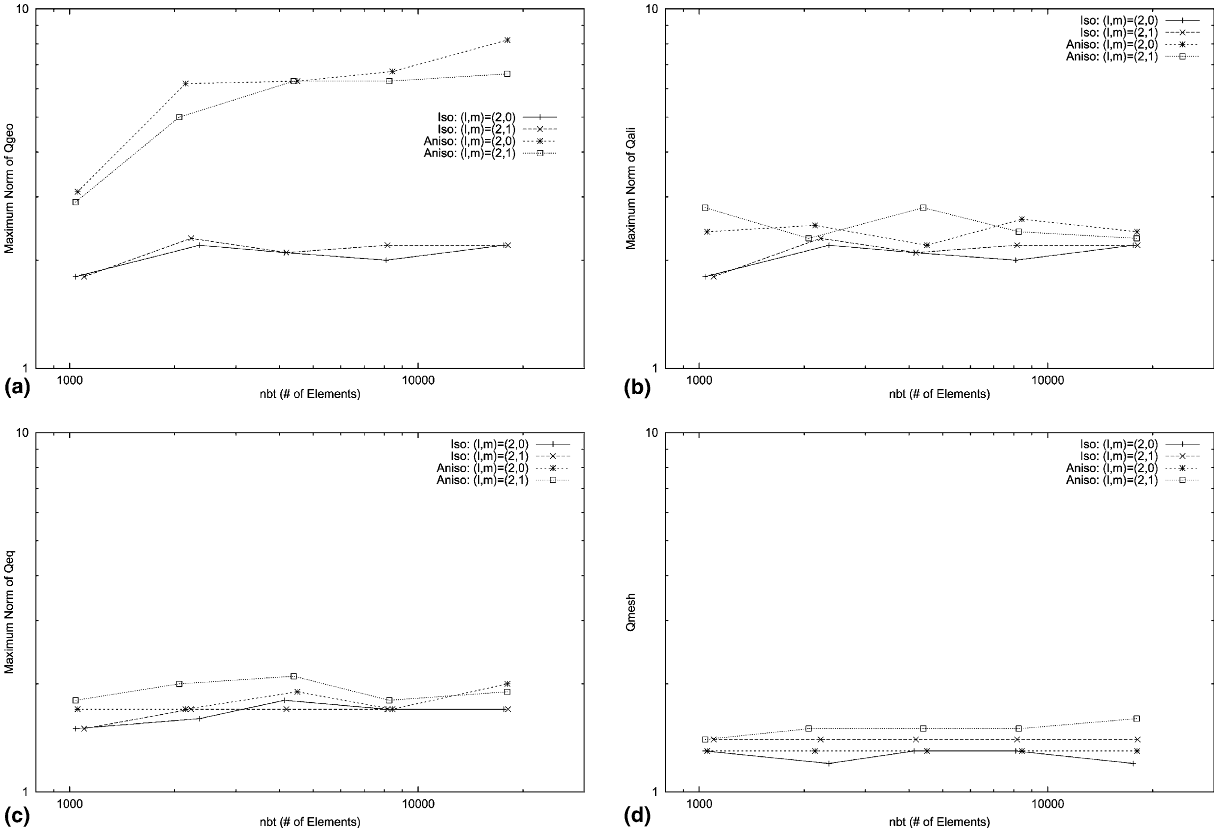

Fig. 15. Example 4.3. The mesh quality measures, $\|Q_{\mathrm{geo}}\|_\infty$, $\|Q_{\mathrm{ali}}\|_\infty$, $\|Q_{\mathrm{eq}}\|_\infty$, and Q_{mesh} are depicted as functions of *nbt* for adaptive meshes generated with various metric tensors.

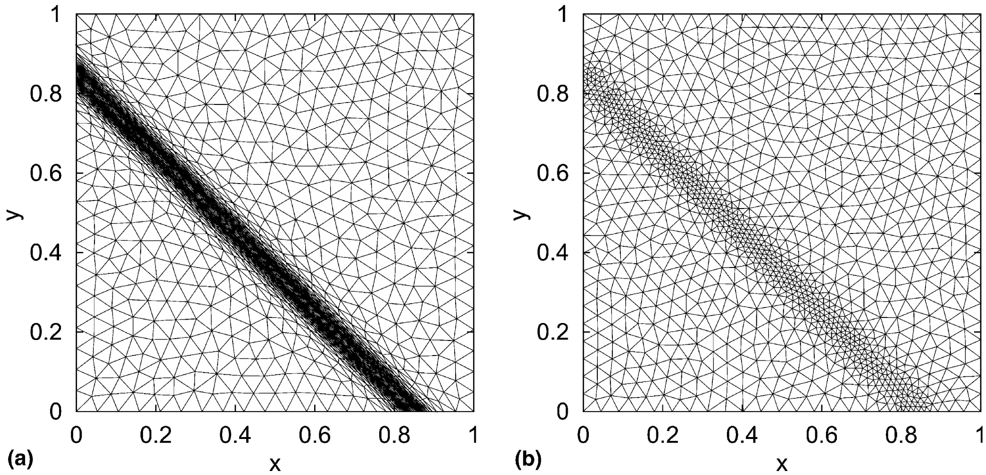

Fig. 16. Example 4.4. (a) An anisotropic mesh obtained with $M_{2,N}$, $(l,m) = (2,1)$, and $N = 1000$: $nbv = 1261$, $nbt = 2388$, $|e|_{H^1} = 0.2$, and $\|e\|_{L^2} = 2.0 \times 10^{-4}$. (b) An isotropic mesh obtained with $M_{3,N}$, $(l,m) = (2,1)$, and $N = 1000$: $nbv = 1214$, $nbt = 2324$, $|e|_{H^1} = 1.1$, and $\|e\|_{L^2} = 3.3 \times 10^{-3}$.

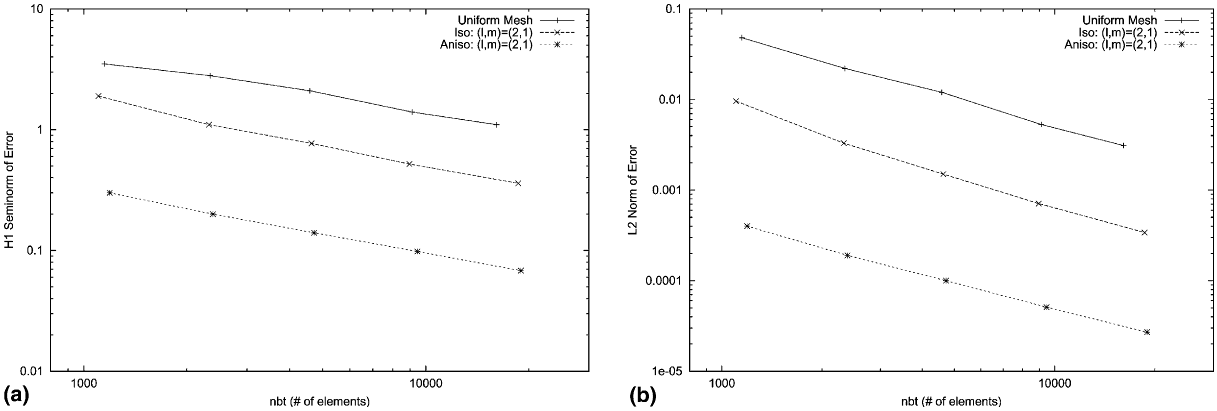

Fig. 17. Example 4.4. The H^1 semi-norm and the L^2 norm are plotted as functions of the number of elements (*nbt*) in (a) and (b), respectively.

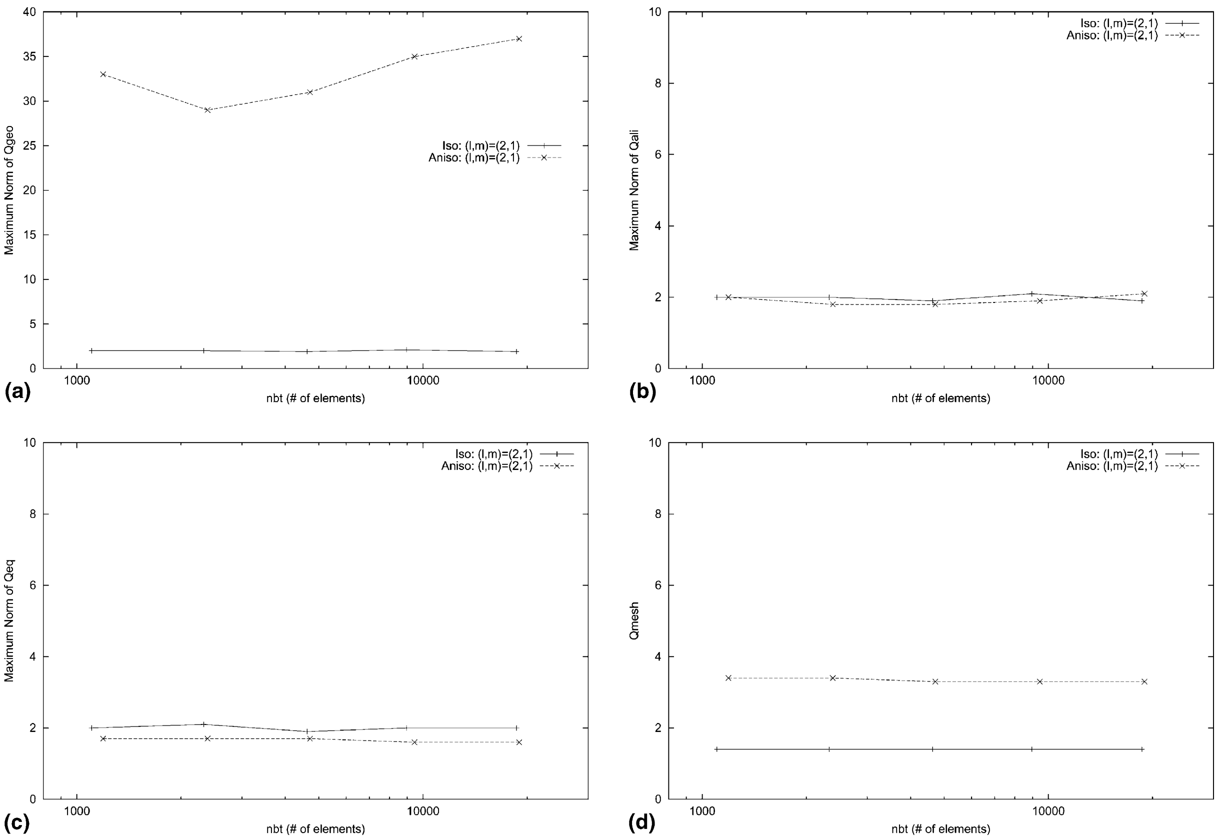

Fig. 18. Example 4.4. The mesh quality measures, $\|Q_{\text{geo}}\|_\infty$, $\|Q_{\text{ali}}\|_\infty$, $\|Q_{\text{eq}}\|_\infty$, and Q_{mesh} are depicted as functions of *nbt* for adaptive meshes generated with various metric tensors.

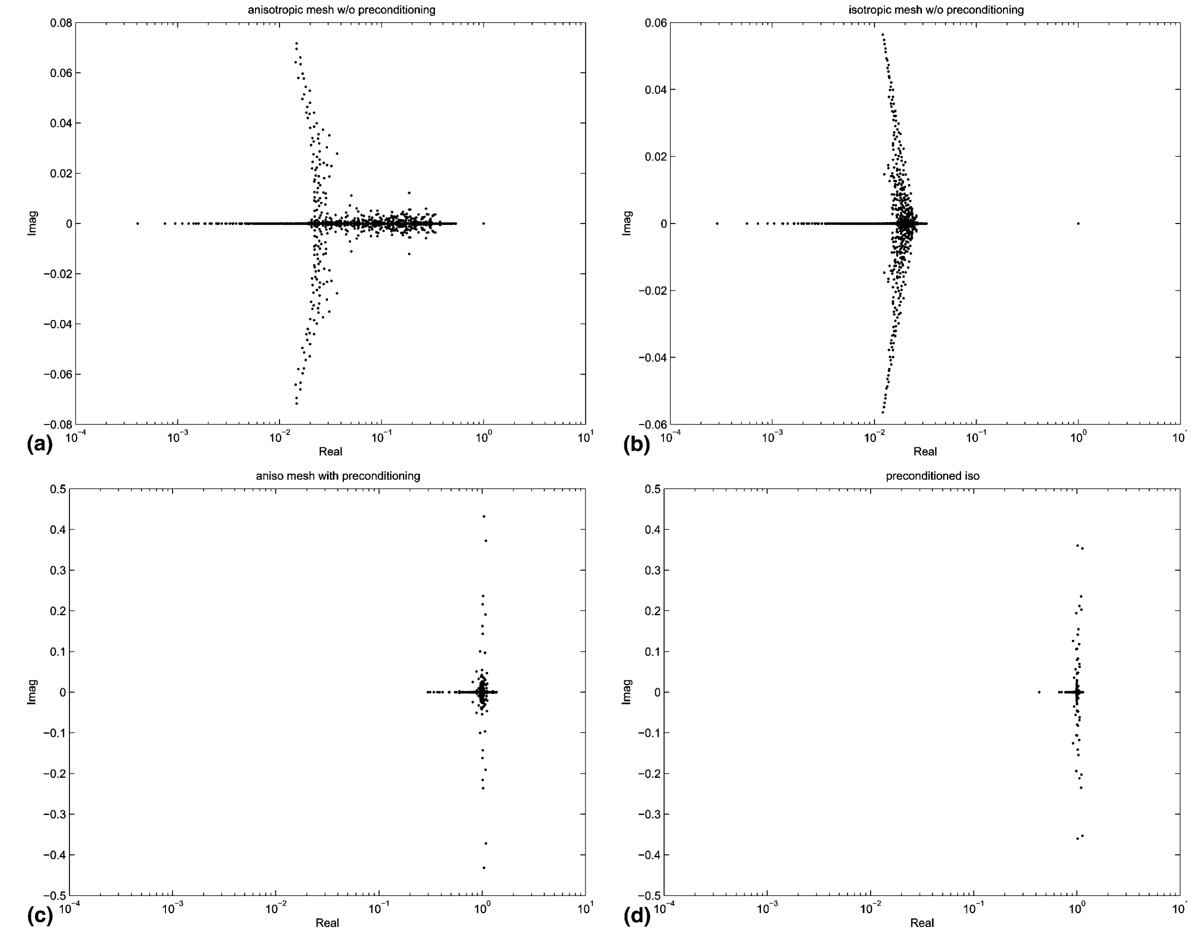

Fig. 19. Example 4.4. Distribution of the eigenvalues of the coefficient matrix resulting from the linear finite element discretization. (a) is for an anisotropic mesh of 1246 vertices; (b) is for an isotropic mesh of 1211 vertices; (c) is for an anisotropic mesh of 1246 vertices but with preconditioning; and (d) is for an isotropic mesh of 1211 vertices but with preconditioning.

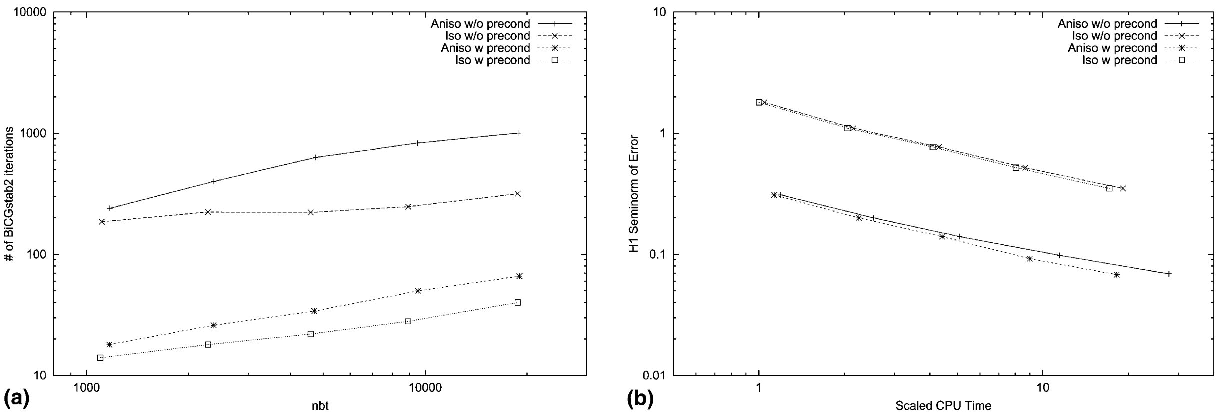

Fig. 20. Example 4.4. (a) The number of BiCGstab2 iterations required to reduce the residual to a level of 10^{-10} for solving a linear algebraic system on a convergent adaptive mesh; (b) The H^1 semi-norm of the error is plotted against the scaled CPU time.

The results in Figs. 19 and 20(a) show that the coefficient matrix has a relatively larger condition number on an anisotropic mesh and its iterative solution requires more BiCGstab2 iterations. But it should be realized that an anisotropic mesh produces a much more accurate solution and thus requires fewer elements to achieve a certain level of accuracy. Overall, it can still be far more efficient to use an anisotropic mesh. To show this, we plot in Fig. 20(b) $|e|_{H^1(\Omega)}$ against the CPU time scaled with the time required for solving the PDE on an isotropic mesh without preconditioning. The improvement in efficiency by using an anisotropic mesh is evident. Interestingly, preconditioning shows only a slight improvement for both isotropic and anisotropic cases.

Example 4.5. This example is to solve the boundary value problem of Poisson's equation

$$-\Delta u = f \quad (x,y) \in \Omega \equiv (0,1) \times (0,1), \tag{90}$$

where the Dirichlet boundary condition and the right-hand side term are chosen such that the exact solution is given by Eq. (89) with ϵ being taken to be 0.005.

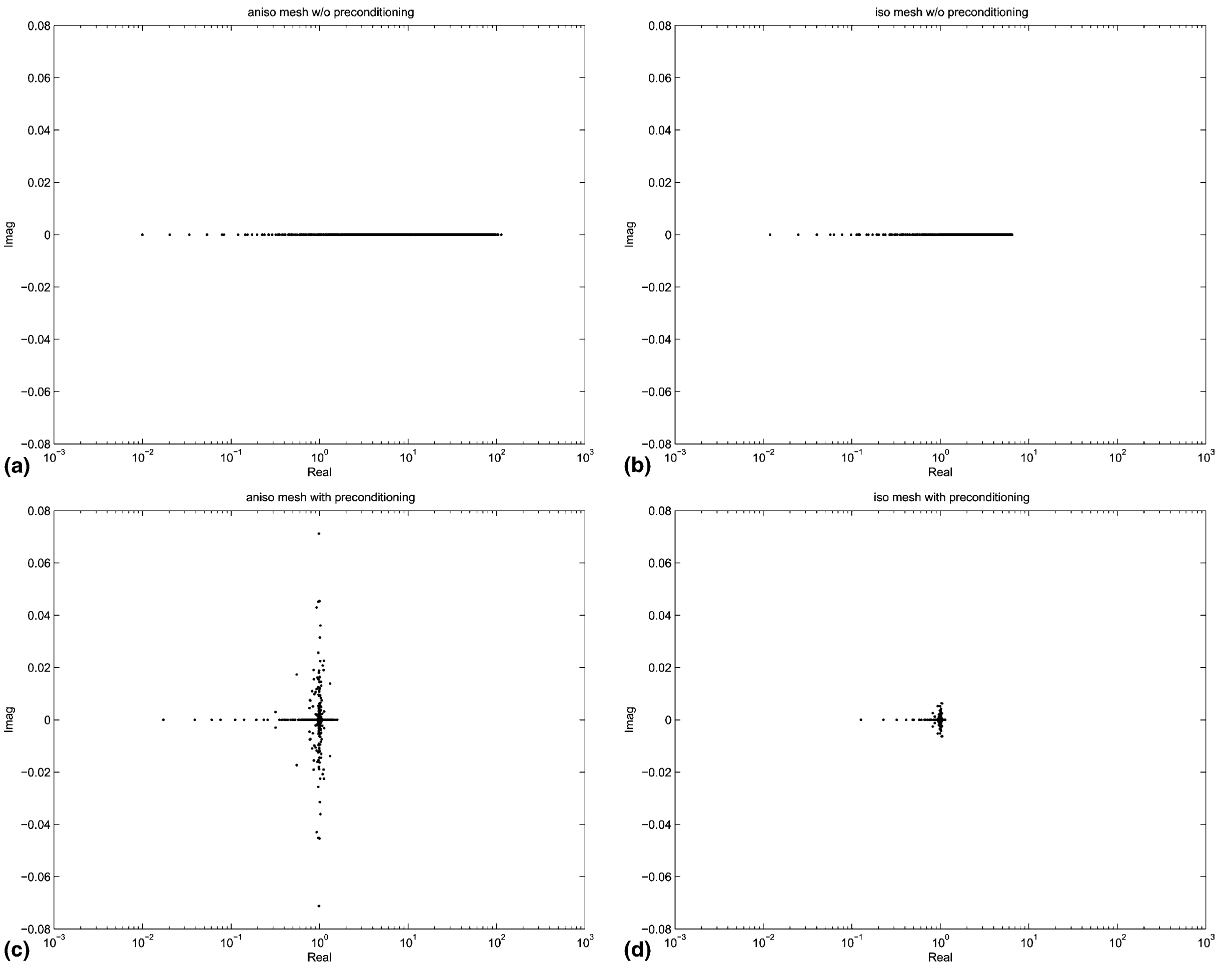

Fig. 21. Example 4.5. Distribution of the eigenvalues of the coefficient matrix resulting from the linear finite element discretization. (a) is for an anisotropic mesh of 1283 vertices; (b) is for an isotropic mesh of 1208 vertices; (c) is for an anisotropic mesh of 1283 vertices but with preconditioning; and (d) is for an isotropic mesh of 1208 vertices but with preconditioning.

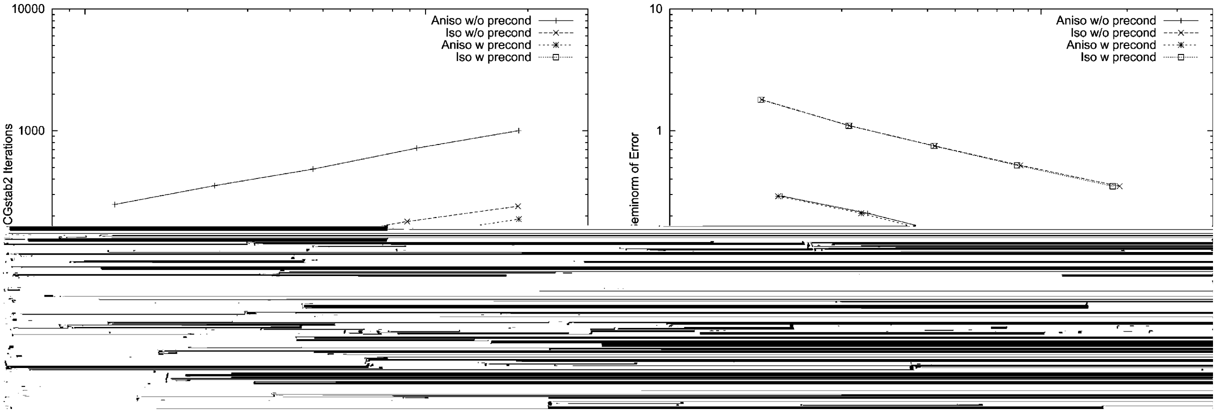

Fig. 22. Example 4.5. (a) The number of BiCGstab2 iterations required to reduce the residual to a level of 10^{-10} for solving a linear algebraic system on a convergent adaptive mesh; (b) The H^1 semi-norm of the error is plotted against the scaled CPU time.

Adaptive meshes, error in the computed solution, and mesh qualities obtained for this example are similar to those for the last example. To save space we do not include them here. Instead, we focus our discussion on the condition of the coefficient matrix resulting from the linear finite element discretization. In Example 4.4, the anisotropic feature of the solution is largely caused by the convection dominated nature of the partial differential equation. Thus, meshes adapting to the solution also adapts, to some extent, to the differential operator in Eq. (88). As a consequence, the condition of the coefficient matrix on an anisotropic mesh should be only slightly worse than that on an isotropic one. On the other hand, the anisotropic feature of the solution of this example is completely caused by the force term. An anisotropic mesh adapting to the solution will not adapt to the Laplacian operator. Thus, one may expect that the condition of the coefficient matrix resulting from an anisotropic mesh is much worse than that on an isotropic mesh. To see how serious this effect is, we plot the distribution of eigenvalues in Fig. 21. The condition number of the coefficient matrix on the anisotropic mesh is about 10 times larger than that on the isotropic mesh, worse than that in the previous example (cf. Fig. 19). But, surprisingly, the situation is not that serious as expected. The required number of the BiCGstab2 iterations and the H^1 semi-norm of the error (as function of scaled CPU time) are plotted in Fig. 22. Once again, the ILU preconditioner is effective in reducing the required number of BiCGstab2 iterations. In addition, the advantage of using an anisotropic mesh over an isotropic mesh is also clear from Fig. 22(b).

5. Conclusions

In the previous sections we have developed a formula for the metric tensor for use in anisotropic mesh generation. The development is based on anisotropic error estimates for polynomial preserving interpolation on simplicial elements. The metric tensor is formulated in terms of either a prescribed number of elements or a prescribed level of interpolation error. It is given in a continuous form in Eq. (68) or (69) for functions of Sobolev space $W^{1,p}(\Omega)$ and in Eq. (70) or (71) for functions of $W^{l,p}(\Omega)$ with $2 \leqslant l \leqslant k+1$ and k being the degree of interpolation polynomials. The formula is general, valid for any $W^{m,q}$ $(0 \leqslant m \leqslant l)$ semi-norm of the interpolation error and any spatial dimension.

The numerical results presented in Section 4 for a select of problems have shown that the defined metric tensor, when used with an existing meshing strategy, is able to produce an anisotropic mesh with correct mesh concentration and good overall quality. They have also demonstrated that significant improvements in accuracy and efficiency can be gained when a properly chosen anisotropic mesh is used for the numerical solution of problems exhibiting anisotropic solution features. The condition of the coefficient matrix resulting from the linear finite element discretization of a PDE on an anisotropic mesh was also addressed. The numerical results suggested that the condition number of the matrix on an adequately chosen anisotropic mesh is relatively larger but not vitally larger than that on an isotropic one, at least for the examples considered. Moreover, an incomplete LU preconditioner with level-one fill-ins is shown to be effective in reducing the number of iterations required for solving the corresponding linear system of algebraic equations.

In this paper, we have concentrated our attention on interpolation error. However, as we have seen in the previous sections, the procedure developed here for defining the metric tensor can also be applied to other types of error estimates, such as a posteriori error estimates and estimates for truncation error.

Acknowledgements

The author would like to thank the referees for their very constructive comments. This work was supported in part by the NSF under Grants DMS-0074240 and DMS-0410545 and the University of Kansas General Research Fund.

References

[1] R.A. Adams, Sobolev Spaces, Academic Press, New York, 1975.
[2] D. Ait-Ali-Yahia, G. Baruzzi, W.G. Habashi, M. Fortin, J. Dompierre, M.-G. Vallet, Anisotropic mesh adaptation: towards user-indepedent, mesh-independent and solver-independent CFD. Part II: structured grids, Int. J. Numer. Meth. Fluids 39 (2002) 657–673.
[3] T. Apel, Anisotropic finite elements: local estimates and applications. in: B.G. Teubner, Stuttgart, (Eds.), 1999. Advances in Numerical Mathematics.
[4] T. Apel, M. Dobrowolski, Anisotropic interpolation with applications to the finite element method, Computing 47 (1992) 277–293.
[5] H. Borouchaki, P.L. George, P. Hecht, P. Laug, E. Saletl, Delaunay mesh generation governed by metric specification: Part I. algorithms, Finite Elem. Anal. Des. 25 (1997) 61–83.
[6] H. Borouchaki, P.L. George, B. Mohammadi, Delaunay mesh generation governed by metric specification: Part II. applications, Finite Elem. Anal. Des. 25 (1997) 85–109.
[7] F.J. Bossen and P.S. Heckbert, A pliant method for anisotropic mesh generation. in: Proceedings of the 5th International Meshing Roundtable, Sandia National Laboratories, Albuquerque, NM, 1996. Sandia Report 96-2301, pp. 63–74.
[8] M.J. Castro-Díaz, F. Hecht, B. Mohammadi, O. Pironneau, Anisotropic unstructured mesh adaption for flow simulations, Int. J. Numer. Meth. Fluids 25 (1997) 475–491.
[9] P.G. Ciarlet, The Finite Element Method for Elliptic Problems, North-Holland, Amsterdam, 1978.
[10] E.F. D'Azevedo, Optimal triangular mesh generation by coordinate transformation, SIAM J. Sci. Stat. Comput. 12 (1991) 755–786.
[11] E.F. D'Azevedo, R.B. Simpson, On optimal triangular meshes for minimizing the gradient error, Numer. Math. 59 (1991) 321–348.
[12] M. Dobrowolski, S. Greaf, C. Pflaum, On a posteriori error estimators in the finite element method on anisotropic meshes, Elec. Trans. Numer. Anal. 8 (1999) 36–45.
[13] J. Dompierre, M.-G. Vallet, Y. Bourgault, M. Fortin, W.G. Habashi, Anisotropic mesh adaptation: towards user-indepedent, mesh-independent and solver-independent CFD. Part III: unstructured meshes, Int. J. Numer. Meth. Fluids 39 (2002) 675–702.
[14] L. Formaggia, S. Perotto, New anisotropic a priori error estimates, Numer. Math. 89 (2001) 641–667.
[15] R.V. Garimella and M.S. Shephard, Boundary layer meshing for viscous flows in complex domain. in: Proceedings of the 7th International Meshing Roundtable, Sandia National Laboratories, Albuquerque, NM, 1998, pp. 107–118.
[16] P.L. George, F. Hecht. Nonisotropic grids, in: J.F. Thompson, B.K. Soni, N.P. Weatherill, (Eds.), Handbook of Grid Generation, CRC Press, Boca Raton, 1999. pp. 20-1–20-29.

[17] M.H. Gutknecht, Variants of BiCGstab for matrices with complex spectrum, SIAM J. Sci. Comput. 14 (1993) 1020–1033.
[18] W.G. Habashi, J. Dompierre, Y. Bourgault, D. Ait-Ali-Yahia, M. Fortin, M.-G. Vallet, Anisotropic mesh adaptation: towards user-indepedent, mesh-independent and solver-independent CFD. Part I: general principles, Int. J. Numer. Meth. Fluids 32 (2000) 725–744.
[19] R. Hagmeeijer, Grid adaption based on modified anisotropic diffusion equations formulated in the parametric domain, J. Comput. Phys. 115 (1994) 169–183.
[20] F. Hecht, Bidimensional anisotropic mesh generator, Technical Report, INRIA, Rocquencourt, 1997. Source code: http://www-rocq1.inria.fr/gamma/cdrom/www/bamg/eng.htm.
[21] W. Huang. Measuring mesh qualities and application to variational mesh adaptation. SIAM J. Sci. Comput., (to appear).
[22] W. Huang, W. Sun, Variational mesh adaptation II: error estimates and monitor functions, J. Comput. Phys. 184 (2003) 619–648.
[23] G. Knuert, R. Verfeurth, Edge residuals dominate a posteriori error estimates for linear finite element methods on anisotropic triangular and tetrahedral meshes, Numer. Math. 86 (2000) 283–303.
[24] G. Kunert, A posteriori error estimation for anisotropic tetrahedral and triangular finite element meshes, Technical Report, TU Chemnitz, 1999. Ph.D. Thesis.
[25] G. Kunert, An a posteriori residual error estimator for the finite element method on anisotropic tetrahedral meshes, Numer. Math. 86 (2000) 471–490.
[26] G. Kunert, A local problem error estimator for anisotropic tetrahedral finite element meshes, SIAM J. Numer. Anal. 39 (2001) 668–689.
[27] A. Liu, B. Joe, On the shape of tetrahedra from bisection, Math. Comput. 63 (1994) 141–154.
[28] A. Liu, B. Joe, Relationship between tetrahedron quality measures, BIT 34 (1994) 268–287.
[29] J. Peraire, M. Vahdati, K. Morgan, O.C. Zienkiewicz, Adaptive remeshing for compressible flow computations, J. Comput. Phys. 72 (1997) 449–466.
[30] J. Remacle, X. Li, M.S. Shephard, and J.E. Flaherty, Anisotropic adaptive simulation of transient flows using discontinuous Galerkin methods, Int. J. Numer. Meth. Eng., 2003, accepted.
[31] Y. Saad, Iterative Methods for Sparse Linear Systems, second ed., SIAM, Philadelphia, 2003.
[32] K.G. Siebert, An a posteriori error estimator for anisotropic refinement, Numer. Math. 73 (1996) 373–398.
[33] H.A. van der Vorst, Bi-CGstab: a fast and smoothly converging variant of Bi-CG for the solution of nonsymmetric linear systems, SIAM J. Sci. Stat. Comput. 13 (1992) 631–644.
[34] S. Yamakawa and K. Shimada, High quality anisotropic tetrahedral mesh generation via ellipsoidal bubble packing. in: Proceedings of the 9th International Meshing Roundtable, Sandia National Laboratories, Albuquerque, NM, 2000. Sandia Report 2000–2207, pp. 263–273.
[35] Z. Zhang and A. Naga, A new finite element gradient recovery method: Superconvergence property, SIAM of Sci. Comput. (to appear).
[36] O.C. Zienkiewicz, J.Z. Zhu, The superconvergence patch recovery and a posteriori error estimates. Part 1: The recovery technique, Int. J. Numer. Meth. Eng. 33 (1992) 1331–1364.
[37] O.C. Zienkiewicz, J.Z. Zhu, The superconvergence patch recovery and a posteriori error estimates. Part 2: Error estimates and adaptivity, Int. J. Numer. Meth. Eng. 33 (1992) 1365–1382.